DOI 10.1002/2015GC005879

Geology, sulphide geochemistry and supercritical venting at the Beebe Hydrothermal Vent Field, Cayman Trough

Alexander P. Webber[1], Stephen Roberts[2], Bramley J. Murton[1], Matthew R.S. Hodgkinson[3]

1. *National Oceanography Centre, Southampton, European Way, Southampton, SO14 3ZH, UK.*
2. *School of Ocean and Earth Science, National Oceanography Centre Southampton, University of Southampton, SO14 3ZH, UK.*
3. *National Oceanography Centre Southampton, University of Southampton Waterfront Campus, European Way, Southampton, SO14 3ZH, UK.*

Correspondence to: A. P. Webber, a.webber@noc.soton.ac.uk

Key points

- The Beebe Vent Field is a Au- Cu- and Zn- rich seafloor sulphide deposit
- Mass wasting of sulphide produces a variety of ores and metal contents
- Lower temperature beehive chimneys control gold precipitation

Abstract

The Beebe Vent Field (BVF) is the world's deepest known hydrothermal system, at 4960m below sea level. Located on the Mid-Cayman Spreading Centre, Caribbean, the BVF hosts high temperature (~401°C) 'black smoker' vents that build Cu, Zn and Au-rich sulphide mounds and chimneys. The BVF is highly gold-rich, with Au values up to 93 ppm and an average Au:Ag ratio of 0.15. Gold precipitation is directly associated with diffuse flow through 'beehive' chimneys. Significant mass-wasting of sulphide material at the BVF, accompanied by changes in metal content, results in metaliferous talus and sediment deposits. Situated on very thin (2-3km thick) oceanic crust, at an ultraslow spreading centre, the hydrothermal system circulates fluids to a depth of ~1.8km in a basement that is likely to include a mixture of both mafic and ultramafic lithologies. We suggest hydrothermal interaction with chalcophile-bearing sulphides in the mantle rocks, together with

Received: Apr 24, 2015; Revised: Jul 13, 2015; Accepted: Jul 17, 2015

precipitation of Au in beehive chimney structures, has resulted in the formation of a Au-rich volcanogenic massive sulphide (VMS) deposit. With its spatial distribution of deposit materials and metal contents, the BVF represents a modern day analogue for basalt hosted, Au-rich VMS systems.

Index terms

1034 Hydrothermal systems (0450, 3017, 3616, 4832, 8135, 8424)

3665 Mineral occurrences and deposits

1032 Mid-oceanic ridge processes (3614, 8416),

1050 Marine geochemistry (4835, 4845, 4850)

1065 Major and trace element geochemistry

Keywords

VMS, Hydrothermal, Gold, Piccard, Seafloor, Black smoker

1. Introduction

Seafloor hydrothermal vent sites are widely recognised features of rifting and seafloor spreading in a variety of tectonic settings, including slow and ultra-slow spreading centres [*Beaulieu et al.,* 2013]. In 2010, two hydrothermal vent fields were discovered in the Cayman Trough related to the ultra-slow spreading Mid-Cayman Spreading Centre [*Connelly et al.,* 2012] after the discovery of hydrothermal plumes in the area [*German et al.,* 2010]. These are the Beebe Vent Field (BVF, Figure 1A), and a moderate temperature site on an oceanic core complex, the Von Damm Vent Field. The BVF lies ~3km to the east of the main spreading axis, and is situated on the eastern flanks of an axial volcanic ridge (Figure 1B). At nearly 5000 metres below sea level (mbsl), the BVF is the deepest known hydrothermal site in the world. It hosts two main areas of focused hydrothermal flow at temperatures up to 401°C, and has developed mounds and aprons of sulphide material. The remarkable discovery of hydrothermal venting on the world's deepest spreading centre opens new possibilities for studying hydrothermal circulation and metal mobility under conditions of extreme pressure and temperature. As the BVF fluids exit the seafloor at conditions comparable to the subsurface reaction zone of typical

fast spreading vent sites [*Von Damm* 1985; *Von Damm and Bischoff*, 1987; *Scott* 1997], they may offer a unique insight into processes operating deep beneath shallower sites.

Here, we present results of detailed mapping, sampling, mineralogical and geochemical analyses that reveal the BVF is an auriferous Cu-Zn volcanogenic massive sulphide (VMS) deposit in the making. We show that as a result of the high temperature and low salinity of fluids venting at the BVF, the fluids remain supercritical even at the point of exit from the vent orifice. The resulting precipitated sulphides are unusually auriferous, with up to ~90 ppm gold, which is unprecedented for any active basalt-hosted system. Furthermore, the heterogeneity in gold concentration between focussed-flow chimneys and diffuse-flow beehive chimneys suggests that chimney morphology exerts a strong control on the gold content of seafloor massive sulphide deposits.

2. Methods

Discovered in 2010 [*Connelly et al*. 2012], The *RRS James Cook* returned to the BVF in February 2013 on leg JC82 where it deployed the ROV *Isis* to depths of over 5000m for high-resolution swath sonar and photographic mapping, and sampling of the vent fauna, fluids, sulphides and host rocks. The new swath map together with extensive exploration of the site during four dives, totalling over 90 hours on the seafloor, allowed for a detailed geological characterisation of the BVF and its surrounding fields of pillow lavas and metaliferous sediments. In the more detailed description presented here, we build on previously published work [*Connelly et al*., 2012*; Nye et al*., 2013; *Kinsey and German*, 2014] and keep to established names for hydrothermal vent sites. It should be noted that other works refer to this site using the alias "Piccard", which was given after the discovery of a hydrothermal plume in the area [German et al., 2010]. In this work we use the name "Beebe", following the discovery paper [*Connelly et al.,* 2012], and as listed in the Interridge database. The chimneys described here as "Beebe-125" are also referred to as "Beebe Vents" in other works. Here we use "Beebe-125" and "Hashtag" for clarity and to describe these two distinct sites. A total of thirty-five sulphide samples were recovered from across the BVF (Figure S1), ranging from highly weathered and iron-oxide rich material, to zero-age sulphide chimney and beehive structures. Sulphide samples were dried under infrared heat lamps before being cut for polished thin sections.

These were examined under reflected and transmitted light to establish mineralogy. X-ray diffraction was used to identify gangue minerals and secondary mineral phases. A portion of the sample, between 10 and 100 g depending on sample size, was removed and ground in a tungsten carbide mill. A large enough proportion of each sample was taken in order to avoid the "nugget effect" of gold grains in geological materials, and to provide representative samples. Despite this, the samples are inhomogeneous on the scale of centimetres, and consequently these "bulk" analyses should be approached with caution. Samples were digested using an aqua-regia, HF-HNO_3, HCl technique and ICP-AES and ICP-MS were used to determine bulk major and trace elements in the sulphide samples. Certified geological reference materials (CH-4 and RTS-1) were used to check accuracy, which was determined as 1-10% for certified elements. Precision was assessed from repeated sample digestions and was 0-10%.

3. Results

3.1 Mapping

ROV derived swath sonar mapping (gridded at a resolution of 25cm – Figure S2), together with extensive exploration and sampling, enabled the production of a detailed geological map of the BVF mounds and surrounding terrain (Figure 2); these data were key to locating features at the site. The site is located at the summit of a dome of pillow lavas that forms part of a NE-SW oriented spur to the N-S trending axial volcanic ridge, which is 3.4km to the west. The spur abuts a regional-scale normal fault 1km to the east of the BVF, with a throw of ~400m and strike length of at least 14km. The spur itself is dissected along its length by a prominent normal fault system with a down-throw of up to 13m to the west. This fault defines the eastern boundary of the BVF, beyond which no evidence for hydrothermal activity, active or extinct, was observed. In the southern portion of the BVF the fault zone is marked by a single, 3-10m wide fissure at least 5m deep, whereas in the northern portion the fault splays and the displacement is transferred onto multiple ~3-5m high, talus-covered scarps. On the northern side of the main Beebe Sea sulphide mound a pronounced linear feature in the bathymetry indicates the presence of another splay of the fault as it emerges from beneath the main (eastern) sulphide mound and talus. Surrounding the BVF, pillow basalts comprise several volcanic

domes with no obvious eruption centres which are variably covered in a thin veneer of pelagic sediment up to ~1cm thick.

The BVF comprises at least six discrete sulphide mounds, three of which host active sites of focused fluid venting (Figure 2). The western-most mound (60m wide), located on the western flank of the main pillow lava dome, hosts a cluster of chimneys called 'Beebe-125'(401°C, Figure 3A) and the newly discovered 'Hashtag' vent site (temperature not measured), which are both high temperature black smoker sites. These two sites are situated on a steep north-south trending ridge at the southern margin of the western-most sulphide mound (not atop the mound, as previously reported), with Beebe-125 on the northern end and Hashtag located 10m south and 10m deeper than Beebe 125. This mound also hosts three areas of lower temperature diffuse venting (Figure 2B, hashed areas). One of these is located on the central western flank of the mound, extends to the top of the mound, and is marked by shimmering water, anemones and bacterial mats. The other area of diffuse venting is located on top, and extending across the eastern flank of the mound, and includes a 'white smoker' that vents pale-grey fluids from a crevice in sulphide rubble. This site also hosts large shrimp colonies, indicating other areas of more focussed flow. The extent of these two areas of diffuse venting is not fully understood and indeed they may be joined together. The third area of diffuse venting is known as the 'Hot Chimlets' vent site, and is located on the northern flank of this mound.

The southernmost sulphide mound (60m wide) hosts the 'Beebe Woods' [*Nye et al*., 2013] vent site (Figure 3B), which is situated on the northern margin of the mound adjacent to a steep cliff, and is a high-temperature (up to 354°C) black smoker, beehive [*Fouquet et al.,* 1993] chimney site. These vents lie 60m south of Hashtag. Apart from Beebe Woods, no active hydrothermal activity was observed on the rest of this mound.

The largest and most prominent sulphide mound hosts the Beebe Sea vent site, and is 110-150m wide and 40m tall. The Beebe Sea vent site is a wide area of diffuse venting found on the northern and western flanks of the mound, including 'Shrimp Gully' [*Nye et al*., 2013]. There is no current high temperature, black smoker venting at this site.

Evidence of past hydrothermal activity is widespread, with numerous inactive chimneys located across the entire BVF. Five hydrothermally inactive sites extend the sulphide zone to the

northeast of Hot Chimlets. Four of these sites comprise sulphide mounds and one consists of three distinct ~1m diameter x 3m tall chimneys in close proximity to exposed pillow lavas. A spectacular example, located 50m to the SW of Beebe Woods, is a single, 13m high, 3m wide inactive chimney, 'Tim's Column', sited on a flat area covered by metaliferous sediment. This chimney marks the beginning of a linear trend of inactive hydrothermal structures that develop northwards through Beebe Sea and ending in the centre of the BVF. A further three extinct sulphide chimney sites are located adjacent to the main fault on the north-eastern margin of the BVF.

Currently active high temperature chimneys are built on thick, solid pedestals of sulphide which are comprised of many generations of chimneys (Figure 3C). These solid bases, both active and inactive, are visible on the high resolution swath bathymetry, particularly if shaded for slope angle (Figure S3), as steep scarps within the mounds below which the drape of talus displays a more uniform slope gradient. Immediately below these edifices lie numerous large pieces of broken chimney (Figure 3D). The western margin of the BVF is marked by the steep flank of the lava dome, resulting in significant mass wasting of metaliferous material to the west. This material forms aprons of talus, composed of material ranging in size from ~1m blocks to sand-sized grains, which extend from the main mounds for ~200m (Figure 3E). Beyond this, down slope and to the west, fine metaliferous sediment collects in depressions and flatter areas, extending the deposit for a further ~150m (Figure 3F). The full extent and thickness of these metaliferous sediments remains unknown. The BVF deposit shows extreme asymmetry, with the vent site abutting a 3-13m fault scarp in the east and with thinner aprons of mass-wasted material extending for hundreds of metres to the west (Figure 4).

3.2 Venting and Petrology

The BVF displays two main styles of high temperature venting. At Beebe-125 and Hashtag, the chimneys are slender, with highly focussed venting at the apex of each chimney. This is where the hottest temperatures were measured, at a maximum stable temperature of 401°C at Beebe-125. Locally, beehive diffusers develop near the base of some chimneys. Groups of 5 or more chimneys grow from a common sulphide base, which can be several metres in breadth and height and composed

of amalgamated chimneys (Figure 3C). Samples recovered included whole chimneys just 6cm wide, to undulating sections of fallen chimneys that were tens of centimetres across. All samples of these chimneys show a very similar mineralogy, with chalcopyrite on the interior, grading out to bornite, disseminated chalcocite (Figure 5A), followed by an anhydrite/pyrite mix. The walls of the chimneys are generally 1 to 1.5cm thick, with 1-8mm of chalcopyrite and varying thicknesses of bornite and anhydrite/pyrite. Silica was present in the outer layer in minor quantities. On the very exterior of some chimneys, euhedral dog-tooth calcite crystals occur, which due to retrograde solubility are stable in the warm seawater on the exterior of the chimneys. Fluids vent almost exclusively from the apex of these chimneys and, although the chimney walls generally appear porous (e.g. Figure 5A), the first few millimetres of chalcopyrite have very little pore space and appear relatively impermeable.

At *Beebe Woods*, venting is characterised by clusters of tall "beehive" chimneys, which are consistently 50-100cm wide and up to 30m tall. They have a highly porous structure, with euhedral laths of pyrrhotite growing into open pore space around primary fluid pathways, sometimes with chalcopyrite in proximity to fluid conduits (Figure 5B). Away from fluid pathways, the grain-size decreases to a fine sulphide mud in a framework of dendritic and granular pyrite. Sphalerite is present as larger masses, and as disseminated blebs or rims on pyrite and pyrrhotite throughout the samples. Chalcopyrite is observed as thin bands surrounding high temperature fluid conduits. Small grains (<0.1mm) of chalcopyrite are present as an accessory phase throughout the samples, and sometimes as mm-scale rims to sphalerite, indicating fluctuating temperatures. A wide range of fluids vent from these 'beehive' structures, from relatively high temperature black fluid (measured range 296-354°C) to shimmering clear water. The shimmering water vents from the apex of some chimneys, but also from large areas of the beehive walls. The range of venting temperatures observed is consistent with the lower temperature, more zinc-rich assemblage recorded here compared to the higher temperature chimneys at Beebe-125 and Hashtag. The absence of significant chalcopyrite in these samples is striking, although it may be present in larger quantities deep within the interior of the chimneys, but was not sampled.

In contrast to the vent structures, the mound talus shows various textures and mineralogy which relate to different stages of alteration and recrystallisation. Some samples show evidence of

primary fluid conduits and relict pyrrhotite laths (Figure 5C, D), whereas others are extensively recrystallised with pyrite/marcasite masses surrounding pyrrhotite blebs (Figure 5E) and semi-massive pyrite (Figure 5F). Other samples are composed of a fine, cryptocrystalline sulphidic mud which does not polish apart from disseminated grains and thin veins of pyrite. Chalcopyrite and sphalerite are present as rare, disseminated grains, with sphalerite sometimes occurring in thin bands (Figure 5F). Atacamite and paratacamite, identified by X-ray diffraction, are found on the exterior of some samples, and observed as a green patchy coating on the sulphide rubble on the seafloor.

Five sediment push cores were recovered from the metaliferous sediment that had accumulated in depressions adjacent to the base of the sulphide mounds. One of these cores (sample 206-Z3) preserves a stratigraphy of several layers, each 1-5cm thick, with a coarse sulphide base and a finer oxide top (Figure 6). These appear to have been deposited in a turbidite-like process, with coarser sulphide material deposited first followed by settling from a cloud of finer material. The presence of these sediments only downslope of the mounds, collection in depressions, and not on the surrounding pillow basalts, suggests mass-wasting as the likely depositional process rather than plume fall-out. These sediments are composed almost exclusively of hydrothermal material, with pyrite and minor sphalerite and chalcopyrite at the base of each bed, and iron oxide comprising the finer material on top. The surrounding pillow basalts show only a light dusting of background sedimentation, whereas the hydrothermal sediments can be greater than 30 cm thick, the length of our push-corer.

3.3 Geochemistry

The focussed chimneys at Beebe-125 and Hashtag contain up to 47 wt% Cu and 0.03-0.24 wt% Zn, whereas the beehive chimneys at Beebe Woods contain 0.5-4 wt% Cu and 0.7-14 wt% Zn (Figure 7a, Table 1). These values are consistent with the mineralogy observed at the two sites; Cu-rich at Beebe-125 and Zn-rich at Beebe Woods. The two types of chimney also show differing precious metal concentrations. The focussed chimneys of Beebe-125 and Hashtag show the lowest Au contents (0.5 to 8 ppm), whereas the beehive chimneys have a mean average of 48.8 ppm Au (n = 8) and a highest value of 93.6 ppm (Figure 7b). The beehive chimneys along with most of the mound rubble and the sediment core lie within the “auriferous” domain of the VMS precious metal element classification

[*Hannington et al.,*1999] (Figure 7c). The beehive chimneys also contain substantial silver, up to 500 ppm, with samples having a high overall Au:Ag ratio compared to other seafloor sulphides (Figure 7d). Higher Au:Ag ratios of 0.24 are found only at the Logatchev vent site (Table S2) [*Fouquet et al.,* 2010].

As expected from its mineralogy of mainly Fe-sulphides, the mound talus material contains lower concentrations of base and precious metals compared to their parent chimneys, with copper and zinc both up to around 100x less (Figure 7a). Talus samples can be roughly defined as two groups – those with low Cu but relatively high Zn, and those with very low Zn and low to high Cu. The grouping of these samples indicates that they originally precipitated at the two different types of chimney. Au and Ag are around 10x less compared to the beehive chimneys, however, at an average of 10.9 ppm Au (n = 16), the mound material retains a substantial gold grade.

In contrast the stratified sediment core contains more base metals than the mound talus, with quantities of Cu and Zn appearing to be an average of the two chimney types (Figure 7a). The fact that they are higher in Cu and Zn than the talus suggests they form as a direct result of chimney collapse and are buried rapidly. They also retain high Au and Ag concentrations, again appearing to average the two chimney sites (Figures 7b, c, d).

In comparison to other mid-ocean vent sites (Table S2 and references therein), the BVF samples contain low Ba, Ni and Sb, whereas Fe, Au, Ag, and Au/Ag are high. Co and Se are comparable to mafic-hosted sites but generally lower than ultramafic-hosted. Sn is intermediate between ultramafic and mafic-hosted sites. Both Pb and Cu are within range of both types of vent site.

4. Discussion

4.1 Physical conditions

The physical conditions of hydrothermal circulation and venting at the BVF are highly unusual. The BVF is ~700m deeper than the next deepest known active hydrothermal site, at 13ºN on the Mid-Atlantic Ridge [*Beltenev et al.,* 2003] (Figure 8a), and also records some of the highest sustained vent fluid temperatures. With a salinity of ~2.3 wt.% (375 mM Cl, Table S1), at ~401°C and ~500 bar, the

venting fluid at BVF is within the supercritical domain of the NaCl-H_2O system (Figure 8a). The Br:Cl ratio of the BVF fluids is higher than seawater (1.55×10^{-3}), at 1.73×10^{-3}, which together with the low salinity, indicates phase separation and Cl partitioning into a brine phase [*Campbell and Edmond*, 1989; *Von Damm* 1990]. Fluid samples from all high temperature vent sites, including Beebe Woods, have the same low salinity, suggesting phase separation at depth and the same fluid upwelling beneath all active high temperature sites.

Phase separation at this depth would require temperatures of at least ~500°C; 100°C hotter than the venting temperature (Figure 8a). In order to intersect the phase boundary, the fluid must be much hotter at depth, and so must have cooled significantly before venting. Shallower hydrothermal vent systems are restricted in temperature by the phase boundary [*Bischoff and Rosenbauer*, 1984], but at the BVF, the venting temperature is consistent with predictions that the maximum temperature of venting is limited to about 400°C by the nonlinear thermodynamic properties of water at 400-600°C [*Jupp and Schultz* 2000, 2004]. Numerical modelling also demonstrates that deeper systems should vent fluids at about 400°C and 2 wt.% NaCl, with brine segregation and retention close to the magmatic source [*Coumou et al.,*2009].

The crust at the Mid-Cayman Spreading Centre is thought to be exceptionally thin, with the basaltic layer described as only a few hundred metres thick, and the overall thickness of the crust, including plutonic assemblages, may be only 2-3km [*Stroup and Fox* 1981; *ten Brink et al.,*2002]. To better understand the depth of hydrothermal circulation, Si and Cl concentrations are often used as a geothermobarometer [e.g. *Foustoukos and Seyfried*, 2007], based on the assumption that Si concentration is controlled by quartz dissolution at higher temperatures. Here, we take an approach similar to *Fontaine et al.*[2009]. BVF fluids show an end-member Si concentration of 24 mmol/kg (Figure 8b). Since the fluid is phase separated, it must have encountered the vapour + liquid phase boundary. Assuming Si concentrations reach equilibrium at depth, the point where the 24 mmol/kg $Si_{(aq)}$ isopleth intersects the phase boundary may be taken as the P-T condition of the reaction zone, which corresponds to 680 bar and 550°C, respectively (Figure 8a). Assuming hydrostatic pressure, this indicates roughly 1.8km to the reaction zone and requires an average geothermal gradient of 90°C/km. The majority of this cooling is expected to occur at depth, where steep geothermal gradients

are indicated from numerical modelling [e.g. *Coumou et al.,*2009; *Hasenclever et al.,* 2014]. Fluid inclusion and oxygen isotope geothermometry beneath the TAG and PACMANUS hydrothermal systems suggest much lower geothermal gradients close to the seafloor [*Petersen et al.,*1998; *Vanko et al.,*2004; *Webber et al.,*2011]. A depth of 1.8 km for hydrothermal circulation beneath the BVF is many times the thickness of basaltic crust at the Mid-Cayman Spreading Centre, and approaches the estimated total thickness of the crust. Volcanically active portions of ultra-slow spreading ridges are thought to generate crust by the emplacement of discrete magma bodies in upper mantle lithologies [*Cannat et al.,*1997, 2006; *Yi et al.,*2014]. This is consistent with samples recovered by submersible traverses of the Cayman Spreading Centre rift walls, which recovered heterogeneously distributed basaltic, gabbroic and ultramafic lithologies, with no clear crustal structure [*Stroup and Fox* 1981]. As such, circulating fluids beneath the BVF may interact with both gabbroic rocks and ultramafic lithologies of the lower crust. Whilst the high silica content of the BVF fluids is uncharacteristic of ultramafic-hosted systems [*Edmonds* 2010], silica equilibration should still occur as the fluids interact with the gabbroic portions of the basement. High H_2 concentrations of as much as 20 mmol/kg [*Seewald et al.,* 2012] do suggest the presence of ultramafic assemblages [*Allen and Seyfried*, 2003], although recent modelling suggests high H_2 concentrations could result from interaction with basalts at higher temperatures (>500°C), with the amount of H_2 in the fluid dependant on temperature and the water-rock ratio [*McDermott* 2015]. The low Cu+Zn average of the BVF sulphides is comparable to mafic hosted systems [Table S2], whilst the Co and Ni content is low compared to ultramafic-hosted systems. However, Sn concentrations are intermediate between mafic- and ultramafic-hosted vents, as is the Zn/Cd ratio of 379, compared to 304 for the average of MORB sites and 614 for the average of ultramafic-hosted sites [*Fouquet et al.* 2010]. Au/Ag ratios are substantially higher than mafic systems and amongst the average values of ultramafic-hosted systems, with only Logatchev being higher [*Fouquet et al.* 2010; *Wang et al.,* 2014]. The low Ni, high Sn and high Au are comparable to the Kairei system, where some portion of the basement was inferred to be ultramafic [*Wang et al.,* 2014]. We suggest the presence of ultramafic lithologies to some degree is likely, given the exceptionally thin basaltic crust, the depth of hydrothermal circulation, ultra-slow spreading rate and high H_2 content of the fluids. The high Au/Ag ratios, similar to other ultramafic-hosted systems, suggest that

these ultramafic lithologies may exert a control on the Au content of the deposit, as has been suggested for conventional ultramafic-hosted deposits [*Fouquet et al.,* 2010]. Alternatively, the genesis of ultramafic-hosted systems and high Au contents could be produced from the same underlying cause, such as slow spreading rate.

4.2 Mass-wasting, galvanic interaction and VMS formation

The base-metal content of the mound rubble at the BVF is much lower than the active chimneys, with only accessory quantities of sphalerite and chalcopyrite present. The clustering of the talus samples into high zinc and high copper groups indicate their origin at the two different vent sites, and subsequent loss of Cu and Zn, or that these samples never contained high quantities of Cu and Zn. The former case suggests that leaching and/or preferential dissolution of Cu-sulphides and sphalerite has occurred. Such changes in mineralogy can be explained by galvanic interaction between sulphide phases [e.g. *Liu et al*.,2008], where the rate of leaching of Cu and Zn is substantially increased when chalcopyrite and sphalerite are in contact with pyrite [*Mehta and Murr,* 1983]. Chalcopyrite in particular was rarely seen in direct contact with pyrite in the mound talus (Figure 5F). The rarity of these base metal sulphides and the 100x reduction in base metal content seen in the mound talus compared to zero-age chimneys (Figure 7A) suggest this process occurs rapidly, leaving little base metal to be incorporated into the deposit on burial of the talus. The dissolution of Cu-sulphides has been linked to the formation of atacamite and paratacamite gossans at TAG [*Hannington* 1993]. Whilst we do find these phases on the exterior of some talus blocks at the BVF, they do not occur as extensive gossans, perhaps due to ongoing sediment transport downslope.

This loss of base metals raises questions with respect to the overall grade and tonnage of the resulting VMS deposit and the release of base metals into the ocean. Collapse of a chimney immediately places the ore sulphides into oxidising conditions under which they not stable. If a large proportion of the Cu- and Zn- bearing minerals are lost from the talus material, then most of the overall grade of the deposit must come from sub-seafloor precipitation, talus that remains proximal to venting and is buried quickly, or chimney structures that do not collapse but are overgrown and incorporated into the mound *in-situ*. Individual vent sites within the field need to be long-lived in

order to build a sufficient mound suitable for the preservation of the ore minerals. Instead of being a primary ore material, the role of altered talus may be to provide a high permeability framework into which ore sulphides can later be precipitated as it is buried and incorporated into the interior of the mound, as part of the "zone refining" model of *Eldridge et al*. [1983]. This variety in precipitation, mass-wasting, alteration, burial and re-precipitation processes is consistent with the ore textures observed in VMS deposits, from preserved chimneys and brecciated primary chimney sulphides to sulphide sands and brecciated pyrite clasts cemented by ore sulphides [e.g. *Eldridge et al*., 1983; *Brown and McClay*, 1998; *Galley et al*., 2007].

The steep topography at the BVF facilitates rapid transport by mass wasting of material away from the active hydrothermal vent site. It is unlikely this material will contribute in a significant way to the base metal content of the deposit unless individual mass wasting events are thick enough to effectively bury ore phases and isolate them from seawater. Instead, mass wasting would produce lenses of massive pyrite/pyrrhotite with a reduced base metal content (Figure 9), although they could retain economically interesting grades of precious metals. These lenses are equivalent to the copper-poor pyrite breccias seen on the exterior of the TAG mounds [*Hannington et al.,* 1998] and at other sites.

Another mass-wasting product at Beebe is the fine metaliferous sediment found at the bottom of the talus slopes and filling depressions that, in one core, shows stratified layers resembling turbidite deposits (Figure 6). This suggests formation by rapid deposition and burial, following the collapse and mass wasting of chimneys which facilitates transport of finer material in a mass-density current. These sediments are not as depleted in base metals as the talus material, instead they appear to average Cu and Zn concentrations from the two types of vent structure (chimneys and beehives). Metal loss from these fine sediments must occur at a much slower rate than from the talus material, perhaps due to their lower permeability, and it is likely that these deposits would represent an economically interesting horizon if preserved in the geological record. These fine sulphidic sediments are equivalent to distal ores preserved in VMS deposits, for example at Yaman Kasy in the southern Uralides, where ores with rhythmic oxide/sulphide bands can be found [*Herrington et al.,*2005].

4.3 Metal content

None of the BVF samples contain any significant Pb mineralisation, and as such, the BVF can be classified as a Cu or Cu-Zn VMS deposit [after *Large*, 1992]. The best estimate of the overall Cu:Zn ratio may come from the metaliferous sediments, which appear to reflect the average of the different types of chimneys and their compositions, at 69-85% Cu (Cu/Cu+Zn+Pb). Such copper-rich deposits are typical of a low tonnage, mafic-dominated VMS [e.g. *Galley et al.,* 2007].

The BVF sulphides are some of the most Au-rich that have been recovered from the seafloor and exhibit high Au to base metal ratios (Figure 10). The mound talus in particular, is extremely Au-rich compared to base metals, likely resulting from the leaching of base metals into seawater. The metaliferous sediments and Beebe Woods chimneys have the highest Au grade, comparable to some of the most Au-rich VMS deposits (Figure 10). The Beebe Woods chimneys in particular are also rich in Ag, although the deposit has a low Ag:Au ratio overall (Figure 7d).

To better understand the likely metal content of Beebe requires a calculation of overall tonnage. We calculated the grade and tonnage of the Beebe mounds and talus material using a volume estimation of the sulphide material that lies above the level of the pillow basalts. We acknowledge there is presumably a mineralised stockwork zone beneath the BVF which we have not included but would add some additional tonnage. In addition, VMS deposits in the geological record show grading of metal content, particularly Cu/Zn ratio, from the surface to the interior, culminating in a Cu-rich inner mound and stockwork [*Lydon*, 1984], which we cannot account for. There is also considerable variation in Au grades, with seafloor sulphide mounds showing more Au-rich exteriors [e.g. *Hannington et al.,* 1995; *Petersen et al.,* 2003]. We therefore use estimates of total metal content and other parameters (Table 2), based primarily on the fine sediments which appear to average both chimney types. We calculate the BVF metal content to be in the region of 1 million tonnes, with a tentative 22,000 tonnes of copper and 59,000 to 172,000 oz Au. Such values would suggest the BVF is a small VMS in commercial terms but contains a substantial amount of Au for its size.

At the BVF, the same high temperature, low salinity fluid is emitted from two vent sites only 60m apart, Beebe-125 and Beebe Woods, yet one forms Au-rich beehive chimneys while the other is relatively Au-poor (Figure 7B). This strongly suggests that, at the BVF, chimney morphology controls

Au-precipitation and, therefore, the generation of an auriferous VMS. The beehive chimneys at Beebe Woods are highly porous, allowing for a high surface area and greater seawater mixing within the chimney [*Fouquet et al.* 1993]. The pH increase, temperature drop and *f*O2 increase associated with seawater mixing all lead to gold precipitation [e.g. *Stefansson and Seward,* 2004; *Pokrovski et al*., 2015]. These rapid changes in fluid chemistry together with the high surface area of the chimney interior may facilitate efficient precipitation of precious metals in comparison to chimneys that consist of one primary fluid conduit and maintain low seawater mixing proportions up to the vent orifice. A similar process was recorded for white smoker chimneys at the TAG hydrothermal field, although the interpretation there was that the high Au values result from reworking of Au from the interior of the mound and repeated concentration within the chimneys [*Hannington et al*., 1995]. This repeated processing by chimney structures was thought to lead to an overall Au loss from the system, since each time a proportion of the gold is vented, resulting in a Au-poor deposit. However, we suggest that at Beebe, due to the steep topography, mass wasting rapidly moves material away from hydrothermal activity, resulting in preservation of at least a proportion of the high Au grades.

Another aspect of the BVF that might control chalcophile element concentrations, including gold, is the proximity of upper-mantle ultramafic lithologies. Since mid-ocean ridge basalts are generally sulphur-saturated, they have a limited capacity to dissolve the sulphide blebs in the upper mantle and so chalcophile elements are preferentially retained in the mantle [*Peach et al*., 1990]. This may be particularly important at the Cayman Trough, where the spreading rate is only 11 mm/yr, leading to the generation of one of the lowest melt thicknesses in the world [*White et al*., 2001]. At such a low rate of melt generation, and with a partition coefficient for Au between sulphide and silicate melt of >15,000 [*Peach et al*.,1990], the vast majority of the gold would be expected to be retained in the mantle sulphides. The concentration of gold in the upper mantle is thought to be considerably higher (1 ppb) [*Salters and Stracke,* 2004] than MORB (0.34 ppb) [Webber et al., 2013]. Given our interpretation of the sub-surface at Beebe includes fluid interaction with mafic and ultramafic lithologies at depth, hydrothermal interaction with the sulphides in the upper mantle rocks provides an alternative mechanism for the release of chalcophile elements.

Most Au-rich VMS deposits in the geological record are associated with a bi-modality in host-rock composition in a back-arc or arc setting, or show evidence for shallow formation resulting in boiling, or have been deformed leading to significant post-depositional enrichment in Au [*Dube et al*., 2007; *Mercier-Langevin et al*., 2011]. The BVF fulfils none of these associations yet is auriferous. However, there is growing evidence that vent sites situated on slow-spreading mid-ocean ridges, especially those ultramafic hosted, are particularly gold-rich [*Münch et al.,* 2001; *Tao et al.,* 2011; *Nayak et al.,* 2014; *Fouquet et al.,* 2010; *Wang et al.,* 2014]. In this geotectonic setting, we suggest the availability of gold-rich sulphide blebs in the reaction zone and, vitally, the precipitation of gold in beehive chimney structures has enabled the formation of an auriferous sea floor massive sulphide deposit.

5. Summary

The BVF is a basalt-hosted hydrothermal system with several unusual and interesting characteristics. It is hosted in an ultra-slow, ultra-deep spreading centre with exceptionally thin basaltic crust, and vents phase separated, low-salinity, supercritical fluid. It is one of only two sites at this time known to vent supercritical fluid, the other being Turtle Pits at 5°S on the Mid-Atlantic Ridge [*Koschinksy et al.,* 2008]. One of the most striking features and on-going processes at the BVF is the steep topography and the influence this has on the growth of the mound and preservation of the deposit (Figure 4). This shows that topography alone can have a significant impact on the metal content and mineralogy of a sulphide mound and therefore VMS deposits in general. We also show that the BVF is an exceptionally Au-rich hydrothermal deposit. Au precipitation at the BVF appears to be controlled by chimney morphology, while the presence of gold-rich sulphide blebs in the reaction zone may increase the overall availability of gold. The tectonic setting, host rock and depth are not thought to be conducive to forming Au-rich VMS deposits in the geological record. The observation that two different chimney sites, just 60m apart, venting the same fluid but precipitating assemblages with highly contrasting Au concentrations mirrors observations from VMS districts, where the Au content of neighbouring deposits can be similarly contrasting [*Hannington et al*., 1999; *Mercier-*

Langevin et al., 2011]. In these ways, Beebe offers an important insight into the formation of sulphide deposits, both past and present, as well as processes of hydrothermal circulation beneath the seafloor.

6. Conclusions

The BVF hosts high temperature, low salinity venting that is supercritical at the vent orifice. Phase separation occurs at depth, with Si and Cl concentrations indicating reaction zone P-T conditions of 680 bar and 550°C.

The high temperature, focussed-flow hydrothermal chimneys are composed of a copper-dominated chalcopyrite/bornite assemblage, while the diffuse-flow hydrothermal 'beehives' are rich in Zn, Au and Ag. Precious metal concentrations in the precipitates are controlled by chimney morphology, where beehive chimneys allow increased seawater mixing within the chimney structure and subsequent precipitation of gold.

The mound talus has lost the majority of its base-metal content to the ocean as a result of galvanic interaction between sulphide phases and oxidised seawater. This has left the talus almost entirely composed of pyrite, with copper and zinc secondary phases such as paratacamite on the exterior of some samples. The talus does retain some precious metal content.

The fine metaliferous sediments contain higher concentrations of both base and precious metals than the mound talus, and appear to represent an average composition of the main high temperature vent sites. The lack of significant pelagic sediment input results in distal hydrothermal sediments containing ore-grade levels of metals.

The BVF represents a mafic-dominated, highly auriferous, Cu-Zn VMS deposit in the making. Its unusually high gold content and high Au:Cu ratios are comparable to some of the most gold-rich VMSs known in the geological record.

Acknowledgments

This study was funded by the Natural Environment Research Council (NERC), UK, Grant NE/101442X/1. We gratefully acknowledge NERC staff and scientists aboard the RRS James Cook. We are grateful for the detailed and insightful comments of the reviewers Sven Petersen and an

anonymous reviewer. Geochemical data used in this study is available in Table 1 and Table S1. Further information about samples available on request. Bathymetry data products available in supporting information.

References

Allen, D. E., and W. E. Seyfried (2003), Compositional controls on vent fluids from ultramatic-hosted hydrothermal systems at mid-ocean ridges: An experimental study at 400 degrees C, 500 bars, *Geochimica Et Cosmochimica Acta*, *67*(8), 1531-1542.

Beaulieu, S. E., E. T. Baker, C. R. German, and A. Maffei (2013), An authoritative global database for active submarine hydrothermal vent fields, *Geochemistry Geophysics Geosystems*, *14*(11), 4892-4905.

Beltenev, V., A. Nescheretov, V. Shilov, A. Shagin, T. Stepanova, G. Cherkashev, B. Batuev, M. Samovarov, I. Rozhdestvenskaya, and I. Andreeva (2003), New discoveries at 12 58' N, 44 52' W, MAR: Professor Logatchev-22 cruise, initial results, *InterRidge News*, *12*(1), 13-14.

Bischoff, J. L., and R. J. Rosenbauer (1984), The Critical-Point and 2-Phase Boundary of Seawater, 200-500-Degrees-C, *Earth and Planetary Science Letters*, *68*(1), 172-180.

Brown, D., and K. McClay (1998), Sulfide textures in the active TAG massive sulfide deposit, 26 o N, Mid-Atlantic Ridge, in *Proceedings of the Ocean Drilling Program, Scientific Results*, edited by P. M. Herzig, S. E. Humphris, D. J. Miller and R. A. Zierenberg, pp. 193-200.

Campbell, A. C., and J. M. Edmond (1989), Halide Systematics of Submarine Hydrothermal Vents, *Nature*, *342*(6246), 168-170.

Cannat, M., Y. Lagabrielle, H. Bougault, J. Casey, N. deCoutures, L. Dmitriev, and Y. Fouquet (1997), Ultramafic and gabbroic exposures at the Mid-Atlantic Ridge: geological mapping in the 15 degrees N region, *Tectonophysics*, *279*(1-4), 193-213.

Cannat, M., D. Sauter, V. Mendel, E. Ruellan, K. Okino, J. Escartin, V. Combier, and M. Baala (2006), Modes of seafloor generation at a melt-poor ultraslow-spreading ridge, *Geology*, *34*(7), 605-608.

Connelly, D. P., J. T. Copley, B. J. Murton, K. Stansfield, P. A. Tyler, C. R. German, C. L. Van Dover, D. Amon, M. Furlong, N. Grindlay, N. Hayman, V. Huhnerbach, M. Judge, T. Le Bas, S. McPhail, A. Meier, K. Nakamura, V. Nye, M. Pebody, R. B. Pedersen, S. Plouviez, C. Sands, R. C. Searle, P. Stevenson, S. Taws, and S. Wilcox (2012), Hydrothermal vent fields and chemosynthetic biota on the world's deepest seafloor spreading centre, *Nature Communications*, *3*.

Coumou, D., T. Driesner, P. Weis, and C. A. Heinrich (2009), Phase separation, brine formation, and salinity variation at Black Smoker hydrothermal systems, *Journal of Geophysical Research-Solid Earth*, *114*.

Dubé, B., P. Gosselin, P. Mercier-Langevin, M. Hannington, and A. Galley (2007), Gold-rich volcanogenic massive sulphide deposits, *Mineral Deposits of Canada: A Synthesis of Major Deposit-Types, District Metallogeny, the Evolution of Geological Provinces, and Exploration Methods: Geological Association of Canada, Mineral Deposits Division, Special Publication*, *5*, 75-94.

Edmonds, H. N. (2010), Chemical Signatures From Hydrothermal Venting on Slow Spreading Ridges, *Diversity of Hydrothermal Systems on Slow Spreading Ocean Ridges*, *188*, 27-42.

Eldridge, C. S., P. B. J. Barton, and H. Ohmoto (1983), Mineral textures and their bearing on the formation of the Kuroko orebodies, *Economic Geology Monograph*, *5*, 241-281.

Fontaine, F. J., W. S. D. Wilcock, D. E. Foustoukos, and D. A. Butterfield (2009), A Si-Cl geothermobarometer for the reaction zone of high-temperature, basaltic-hosted mid-ocean ridge hydrothermal systems, *Geochemistry Geophysics Geosystems*, *10*.

Fouquet, Y., A. Wafik, P. Cambon, C. Mevel, G. Meyer, and P. Gente (1993), Tectonic Setting and Mineralogical and Geochemical Zonation in the Snake Pit Sulfide Deposit (Mid-Atlantic Ridge at 23-Degrees-N), *Economic Geology and the Bulletin of the Society of Economic Geologists*, *88*(8), 2018-2036.

Fouquet, Y., P. Cambon, J. Etoubleau, J. L. Charlou, H. Ondreas, F. J. A. S. Barriga, G. Cherkashov, T. Semkova, I. Poroshina, M. Bohn, J. P. Donval, K. Henry, P. Murphy, and O. Rouxel (2010), Geodiversity of Hydrothermal Processes Along the Mid-Atlantic Ridge and Ultramafic-Hosted Mineralization: A New Type of Oceanic Cu-Zn-Co-Au Volcanogenic Massive Sulfide Deposit, *Diversity of Hydrothermal Systems on Slow Spreading Ocean Ridges*, *188*, 321-367.

Foustoukos, D. I., and W. E. Seyfried (2007), Quartz solubility in the two-phase and critical region of the NaCl-KCl-H2O system: Implications for submarine hydrothermal vent systems at 9 degrees 50 ' N East Pacific Rise, *Geochimica Et Cosmochimica Acta*, *71*(1), 186-201.

Galley, A. G., M. Hannington, and I. Jonasson (2007), Volcanogenic massive sulphide deposits, *Mineral Deposits of Canada: A Synthesis of Major Deposit-Types, District Metallogeny, the Evolution of Geological Provinces, and Exploration Methods: Geological Association of Canada, Mineral Deposits Division, Special Publication*, *5*, 141-161.

German, C. R., A. Bowen, M. L. Coleman, D. L. Honig, J. A. Huber, M. V. Jakuba, J. C. Kinsey, M. D. Kurz, S. Leroy, J. M. McDermott, B. M. de Lepinay, K. Nakamura, J. S. Seewald, J. L. Smith, S. P. Sylva, C. L. Van Dover, L. L. Whitcomb, and D. R. Yoerger (2010), Diverse styles of submarine venting on the ultraslow spreading Mid-Cayman Rise, *Proceedings of the National Academy of Sciences of the United States of America*, *107*(32), 14020-14025.

Hannington, M. D. (1993), The Formation of Atacamite during Weathering of Sulfides on the Modern Sea-Floor, *Canadian Mineralogist*, *31*, 945-956.

Hannington, M. D., A. G. Galley, P. M. Herzig, and S. Petersen (1998), 28. COMPARISON OF THE TAG MOUND AND STOCKWORK COMPLEX WITH CYPRUS-TYPE MASSIVE SULFIDE DEPOSITS1, paper presented at Proceedings of the ocean drilling program, scientific results.

Hannington, M. D., K. H. Poulson, J. F. H. Thompson, and R. H. Sillitoe (1999), Volcanogenic gold in the massive sulfide environment, in *Volcanic-Associated Massive Sulfide Deposits: Processes and Examples in Modern and Ancient Settings: Reviews in Economic Geology*, edited by C. T. Barrie and M. Hannington, pp. 325-356.

Hannington, M., S. Petersen, P. Herzig, and I. Jonasson (2004), A global database of seafloor hydrothermal systems, including a digital database of geochemical analyses of seafloor polymetallic sulfides, *Gelogical Survey ofCanada, Open File*, *4598*.

Hannington, M. D., M. K. Tivey, A. C. L. Larocque, S. Petersen, and P. A. Rona (1995), The occurrence of gold in sulfide deposits of the TAG Hydrothermal Field, Mid-Atlantic Ridge, *Canadian Mineralogist*, *33*, 1285-1310.

Hasenclever, J., S. Theissen-Krah, L. H. Rupke, J. P. Morgan, K. Iyer, S. Petersen, and C. W. Devey (2014), Hybrid shallow on-axis and deep off-axis hydrothermal circulation at fast-spreading ridges, *Nature*, *508*(7497), 508-+.

Herrington, R., V. Maslennikov, V. Zaykov, I. Seravkin, A. Kosarev, B. Buschmann, J. J. Orgeval, N. Holland, S. Tesalina, P. Nimis, and R. Armstrong (2005), Classification of VMS deposits: Lessons from the South Uralides, *Ore Geology Reviews*, *27*(1-4), 203-237.

Humphris, S. E., and J. R. Cann (2000), Constraints on the energy and chemical balances of the modern TAG and ancient Cyprus seafloor sulfide deposits, *Journal of Geophysical Research-Solid Earth*, *105*(B12), 28477-28488.

Jupp, T., and A. Schultz (2000), A thermodynamic explanation for black smoker temperatures, *Nature*, *403*(6772), 880-883.

Jupp, T. E., and A. Schultz (2004), Physical balances in subseafloor hydrothermal convection cells, *Journal of Geophysical Research-Solid Earth*, *109*(B5).

Kinsey, J. C., and C. R. German (2013), Sustained volcanically-hosted venting at ultraslow ridges: Piccard Hydrothermal Field, Mid-Cayman Rise, *Earth and Planetary Science Letters*, *380*, 162-168.

Koschinsky, A., D. Garbe-Schonberg, S. Sander, K. Schmidt, H. H. Gennerich, and H. Strauss (2008), Hydrothermal venting at pressure-temperature conditions above the critical point of seawater, 5 degrees S on the Mid-Atlantic Ridge, *Geology*, *36*(8), 615-618.

Large, R. R. (1992), Australian volcanic-hosted massive sulfide deposits; features, styles, and genetic models, *Economic Geology*, *87*(3), 471-510.

Liu, Q. Y., H. P. Li, and L. Zhou (2008), Galvanic interactions between metal sulfide minerals in a flowing system: Implications for mines environmental restoration, *Applied Geochemistry*, *23*(8), 2316-2323.

Lydon, J. W. (1984), Ore Deposit Models .8. Volcanogenic Massive Sulfide Deposits .1. A Descriptive Model, *Geoscience Canada*, *11*(4), 195-202.

McDermott, J. M. (2015), Geochemistry of deep-sea hydrothermal vent fluids from the Mid-Cayman Rise, Caribbean Sea, Massachusetts Institute of Technology and WHOI, Cambridge, Massachusetts, USA.

Mehta, A. P., and L. E. Murr (1983), Fundamental-Studies of the Contribution of Galvanic Interaction to Acid-Bacterial Leaching of Mixed Metal Sulfides, *Hydrometallurgy*, *9*(3), 235-256.

Mercier-Langevin, P., M. D. Hannington, B. Dube, and V. Becu (2011), The gold content of volcanogenic massive sulfide deposits, *Mineralium Deposita*, *46*(5-6), 509-539.

Munch, U., C. Lalou, P. Halbach, and H. Fujimoto (2001), Relict hydrothermal events along the super-slow Southwest Indian spreading ridge near 63 degrees 56 ' E - mineralogy, chemistry and chronology of sulfide samples, *Chemical Geology*, *177*(3-4), 341-349.

Nayak, B., P. Halbach, B. Pracejus, and U. Munch (2014), Massive sulfides of Mount Jourdanne along the super-slow spreading Southwest Indian Ridge and their genesis, *Ore Geology Reviews*, *63*, 115-128.

Nye, V., J. T. Copley, and P. A. Tyler (2013), Spatial Variation in the Population Structure and Reproductive Biology of Rimicaris hybisae (Caridea: Alvinocarididae) at Hydrothermal Vents on the Mid-Cayman Spreading Centre, *Plos One*, *8*(3).

Peach, C. L., E. A. Mathez, and R. R. Keays (1990), Sulfide Melt Silicate Melt Distribution Coefficients for Noble-Metals and Other Chalcophile Elements as Deduced from Morb - Implications for Partial Melting, *Geochimica Et Cosmochimica Acta*, *54*(12), 3379-3389.

Petersen, S., P. M. Herzig, and M. D. Hannington (1998), Fluid inclusion studies as a guide to the temperature regime within the TAG hydrothermal mound, 26 N, Mid-Atlantic Ridge, paper

presented at PROCEEDINGS-OCEAN DRILLING PROGRAM SCIENTIFIC RESULTS, NATIONAL SCIENCE FOUNDATION.

Petersen, S., P. M. Herzig, M. D. Hannington, and J. B. Gemmell (2003), Gold-rich massive sulfides from the interior of the felsic-hosted PACMANUS massive sulfide deposit, Eastern Manus Basin (PNG), *Mineral Exploration and Sustainable Development, Vols 1 and 2*, 171-174.

Pokrovski, G. S., N. N. Akinfiev, A. Y. Borisova, A. V. Zotov, and K. Kouzmanov (2015), Gold speciation and transport in geological fluids: insights from experiments and physical-chemical modelling, in *Gold-Transporting Hydrothermal Fluids in the Earth's Crust*, edited by P. S. Garofalo and J. R. Ridley, The Geological Society of London 2014, London.

Salters, V. J. M., and A. Stracke (2004), Composition of the depleted mantle, *Geochemistry Geophysics Geosystems*, *5*.

Scott, S. D. (1997), Submarine hydrothermal systems and deposits, in *Geochemistry of Hydrothermal Ore Deposits (3rd ed.)*, edited by H. L. Barnes, pp. 797-875, Wiley, New York.

Seewald, J., J. McDermott, C. German, S. Sylva, E. Reeves, and F. Klein (2012), Geochemistry of Hydrothermal Fluids from the Ultra-Slow Spreading Mid-Cayman Rise, paper presented at AGU Fall Meeting Abstracts.

Stefansson, A., and T. M. Seward (2004), Gold(I) complexing in aqueous sulphide solutions to 500 degrees C at 500 bar, *Geochimica Et Cosmochimica Acta*, *68*(20), 4121-4143.

Stroup, J. B., and P. J. Fox (1981), Geologic Investigations in the Cayman Trough - Evidence for Thin Oceanic-Crust Along the Mid-Cayman Rise, *Journal of Geology*, *89*(4), 395-420.

Tao, C. H., H. M. Li, W. Huang, X. Q. Han, G. H. Wu, X. Su, N. Zhou, J. Lin, Y. H. He, and J. P. Zhou (2011), Mineralogical and geochemical features of sulfide chimneys from the 49A degrees 39 ' E hydrothermal field on the Southwest Indian Ridge and their geological inferences, *Chinese Science Bulletin*, *56*(26), 2828-2838.

ten Brink, U. S., D. F. Coleman, and W. P. Dillon (2002), The nature of the crust under Cayman Trough from gravity, *Marine and Petroleum Geology*, *19*(8), 971-987.

Vanko, D. A., W. Bach, S. Roberts, C. J. Yeats, and S. D. Scott (2004), Fluid inclusion evidence for subsurface phase separation and variable fluid mixing regimes beneath the deep-sea PACMANUS hydrothermal field, Manus Basin back arc rift, Papua New Guinea, *Journal of Geophysical Research-Solid Earth*, *109*(B3).

Von Damm, K. L. (1990), Seafloor Hydrothermal Activity - Black Smoker Chemistry and Chimneys, *Annual Review of Earth and Planetary Sciences*, *18*, 173-204.

Von Damm, K. L., and J. L. Bischoff (1987), Chemistry of Hydrothermal Solutions from the Southern Juan-De-Fuca Ridge, *Journal of Geophysical Research-Solid Earth and Planets*, *92*(B11), 11334-11346.

Von Damm, K. L., J. M. Edmond, B. Grant, and C. I. Measures (1985), Chemistry of Submarine Hydrothermal Solutions at 21-Degrees-N, East Pacific Rise, *Geochimica Et Cosmochimica Acta*, *49*(11), 2197-2220.

Wang, Y. J., X. Q. Han, S. Petersen, X. L. Jin, Z. Y. Qiu, and J. H. Zhu (2014), Mineralogy and geochemistry of hydrothermal precipitates from Kairei hydrothermal field, Central Indian Ridge, *Marine Geology*, *354*, 69-80.

Webber, A. P., S. Roberts, R. Burgess, and A. J. Boyce (2011), Fluid mixing and thermal regimes beneath the PACMANUS hydrothermal field, Papua New Guinea: Helium and oxygen isotope data, *Earth and Planetary Science Letters*, *304*(1-2), 93-102.

Webber, A. P., S. Roberts, R. N. Taylor, and I. K. Pitcairn (2013), Golden plumes: Substantial gold enrichment of oceanic crust during ridge-plume interaction, *Geology*, *41*(1), 87-90.
White, R. S., T. A. Minshull, M. J. Bickle, and C. J. Robinson (2001), Melt generation at very slow-spreading oceanic ridges: Constraints from geochemical and geophysical data, *Journal of Petrology*, *42*(6), 1171-1196.
Yi, S. B., C. W. Oh, S. J. Pak, J. Kim, and J. W. Moon (2014), Geochemistry and petrogenesis of mafic-ultramafic rocks from the Central Indian Ridge, latitude 8 degrees-17 degrees S: denudation of mantle harzburgites and gabbroic rocks and compositional variation of basalts, *International Geology Review*, *56*(14), 1691-1719.

Tables

Table 1: Bulk rock geochemical analyses for BVF sulphides.

Footnote: Cu, Fe, Zn analysed by ICP-AES and given in wt. %. All other elements analysed by ICP-MS and given in ppm. Sediment samples are taken from the stratified core shown in Figure 6. Samples with missing location data were unidentified fragments of other samples, and designated sample numbers aboard ship.

Table 2: Parameters used in metal content calculation.

Figure Captions

Figure 1.

A: Location of the Beebe Vent Field (BVF) in the Mid-Cayman Spreading Centre, Cayman Trough, and world location map (inset). Position of the BVF is given by the box, which shows the extent of (B). Major faults are displayed in red, located by processing the bathymetry for slope angle, and the spreading axis is shown in black. B: The area immediately surrounding the BVF is composed of hummocky pillow basalt mounds. The BVF is situated on a NE-SW trending spur of lava domes. The mounds and metaliferous talus of the BVF can be seen on the western side of this spur, which is bisected by a fault network. The outline of the bathymetry shown in Figure 2 is given in black

Figure 2.

A: High resolution swath bathymetry, overlain with lithological boundaries and the main features of the Beebe hydrothermal vent field. The black line AB is the line of the cross section shown in Figure 4. B: detailed positions of the main high temperature and several diffuse vent sites. The outline of this pane is shown in A. C: The mapped lithologies from high resolution swath mapping and ground-truthing with the ISIS ROV. "Sediment" refers to metaliferous sediment. The pillow basalts are variably coated with a thin veneer of pelagic sediment and this has not been mapped. "Talus" refers to sulphide talus. The "mounds" outline the solid sulphide edifices which form steep scarps, below which sulphide talus forms more uniformly sloped talus aprons. These scarps are visible on the slope-shaded map (Figure S3).

Figure 3.

A: Beebe-125 showing chimney morphology typical of Beebe-125 and Hashtag sites, looking east. The chimney in the centre of the image is ~30cm wide. B: Beehive chimneys of Beebe Woods looking east. White areas are shrimp, and the darker areas vent fluid that is too hot for the shrimp to colonise. Pictured chimneys are 50-100cm wide. C: Chimneys grow from a block of sulphide comprised of amalgamated extinct chimneys, this view is of Hashtag and is 2m wide, looking north. D: Immediately below active and inactive vent sites are blocks of fallen chimneys, with 10cm laser sights. E: Further downslope from D, blocks of sulphide are no longer recognisable as chimneys, are significantly recrystallised and have lost a lot of their base metal content. Secondary alteration minerals are abundant. 10cm laser sights. F: More distally, fine metaliferous sediment forms thick deposits and drapes pillow lavas, sometimes with a very thin layer of background sedimentation on top, as seen here. 10cm laser sights.

Figure 4:

Cross section and summary of geological processes at the BVF. The section line AB is shown on Figure 2 with the seafloor being the real topography data collected during JC82, without any vertical exaggeration. Inferred solid sulphide mounds are shown in purple, which are defined by a steep gradient of the bathymetry visible on each mound (Figure S3). In pink is the draped mound talus,

which displays a more consistent and gently sloping gradient and undergoes galvanic interaction, leaching base metals into the ocean. In yellow is the finer metaliferous sediment, which collects in depressions, is interbedded with the talus and displays strong stratification with coarse to fine grading within layers. The level of the basalt host rock, given by a dashed line, is inferred.

Figure 5.

Photomicrographs of primary sulphide (A,B) and mound talus (C-F). A: section through the wall of a high temperature chimney, with chalcopyrite grading to bornite and chalcocite in the upper right. To the left, the chalcopyrite continues to the fluid conduit, becoming less porous. B: section of beehive-type chimney from Beebe Woods. Laths of pyrrhotite grow from a porous chalcopyrite wall. The right side of the image is very fine, porous, pyrite, anhydrite and sphalerite. C: A relict fluid conduit in mound talus. Rims of pyrite surround very fine amalgamations of anhydrite and sulphide mud (black areas). D: relict pyrrhotite laths, now replaced with fine sulphide mud, rimmed with pyrite. E: Blebs of pyrrhotite being recrystallised as a pyrite/pyrrhotite mix, with sphalerite. F: Semi-massive pyrite with bands of sphalerite and grains of chalcopyrite. py = pyrite, po = pyrrhotite, mc = marcasite, chc = chalcocite, sph = sphalerite, cpy = chalcopyrite.

Figure 6

Sediment core and log of metaliferous sediments from the BVF. The core shows centimetre-scale stratigraphy with thin, coarse sulphide bases and thicker, finer grained oxide tops. This indicates a turbiditic mode of deposition. Geochemical analysis of this sediment core is given in Table 1.

Figure 7.

Results of bulk geochemical analysis of sulphide samples. In all diagrams closed triangles are of beehive chimneys, open triangles are focussed chimneys, crosses are mound talus and pluses are fine metaliferous sediment. Errors are encompassed by the symbol size. A: Cu vs Zn.The two chimney types display very different base metal contents, with the focussed chimneys being rich in Cu whilst the beehive chimneys are rich in Zn. The mound talus show lower base metal contents, and are

arranged in arrays which suggest which type of chimney they originated from. Fine sediment averages the two chimney sites. B: Cu vs Au. The beehive chimneys show by far the highest Au content, with the fine sediment second and the mound talus third. The talus retains economically interesting Au levels despite massive loss of base metals. C: Precious metal discrimination diagram after *Hannington et al*., [1999]. Most samples except four of the focussed chimney, 4 talus and one fine sediment samples lie in the "auriferous" domain of the graph. D: Ag vs Au, with the grey dots being the available data for seafloor sulphide precious metal content, compiled by *Hannington et al*., [2004]. The BVF samples display very high Au:Ag ratios, with some of the highest Au values ever recorded for seafloor sulphides, and Ag values which are well above average in the beehive chimneys

Figure 8.

A: Temperature-pressure diagram for the H_2O-NaCl system with the phase boundary for 3.2 wt% NaCl plotted. Grey triangles are the P-T conditions for known hydrothermal systems, from the Interridge database [*Beaulieu et al*., 2013]. Compared to other high temperature systems, the BVF lies far from the phase boundary, indicating the temperature of venting fluids are not constrained by the phase boundary as at shallower sites. The star is the critical point for H2O-NaCl at 2.3 wt% NaCl, the composition of BVF fluids, which is ~283 bar and ~399°C. At 401-403°C, the BVF are 2-4 degrees hotter than the critical point and are thus supercritical. Also shown is the isopleth for silica dissolution at 24 mmol/kg, the end-member composition of BVF fluids (shown in B). Based on the observation that the BVF fluids are phase-separated, the fluid must have existed on the phase boundary at depth. The intersection of the phase boundary with the 24 mmol/kg Si isopleth suggests equilibrium at ~680 bars and ~550°C. B: Mg vs Si of BVF fluids. The star is bottom sea-water. Since Mg in the end-member is assumed to be 0, the end-member fluid Si concentration is 24 mmol/kg. Fluid chemistry data given in Table S1.

Figure 9.

Conceptual model for the influence of steep topography on VMS deposit formation, as indicated by observations from the BVF. A: A sulphide deposit on flat topography builds a mound in layers that are successively buried. Diffuse venting from the mound, which is suggested to constitute to 70% of total fluid flux [*Humphris and Cann*, 2000], keep Cu- Zn- and Pb- sulphide phases in more stable conditions, whilst precipitating ore phases which cement the talus clasts. Consequently, the mound talus represents a significant proportion of the base metal content of the deposit. B: With steep topography, a large proportion of the mound talus is rapidly transported away from higher temperature conditions, including diffuse venting, placing it under conditions in which sulphide phases can rapidly dissolve and undergo galvanic interaction. The mound talus loses the majority of its base metal content. Mass-density currents deposit finer metaliferous sediments in a distal setting, and burial is fast enough to preserve base metals. C: The resulting VMS deposit constitutes a sulphide lens and stockwork, which are the main ore body, but the lens is smaller than it would have been on gentler terrain. Adjacent, down-dip, is a massive pyrite lens which is barren of base metals but may preserve precious metal content. More distally are metaliferous sediments, which will vary in composition due to background sediment influx. The final grade of these fine sediments depends on the ratio of metaliferous to background sedimentation.

Figure 10:

Au vs total base metal content (Cu + Zn + Pb in wt. %). Symbols as in Figure 7, with the grey dots being global VMS deposits in the geological record. Diagram after *Mercier-Langevin et al*., [2011]. Auriferous domains are defined either as having a greater gold grade than the geometric mean + geometric standard deviation of all VMS deposits, which is 3.46 ppm, or by having a greater Au content in ppm than total base metal content in wt. %. Only a handful of VMS deposits lie in either of these auriferous domains. Almost all of the BVF lie in the auriferous domain of the diagram, with most having a greater Au grade than total base metal content. The average of all BVF samples is given by the star. Although this compares hand specimen-scale samples to whole deposits, it gives an indication that the resulting deposit as a whole would be auriferous. In particular, the Au:base metal ratio of the mound talus is exceptionally high due to base metal loss.

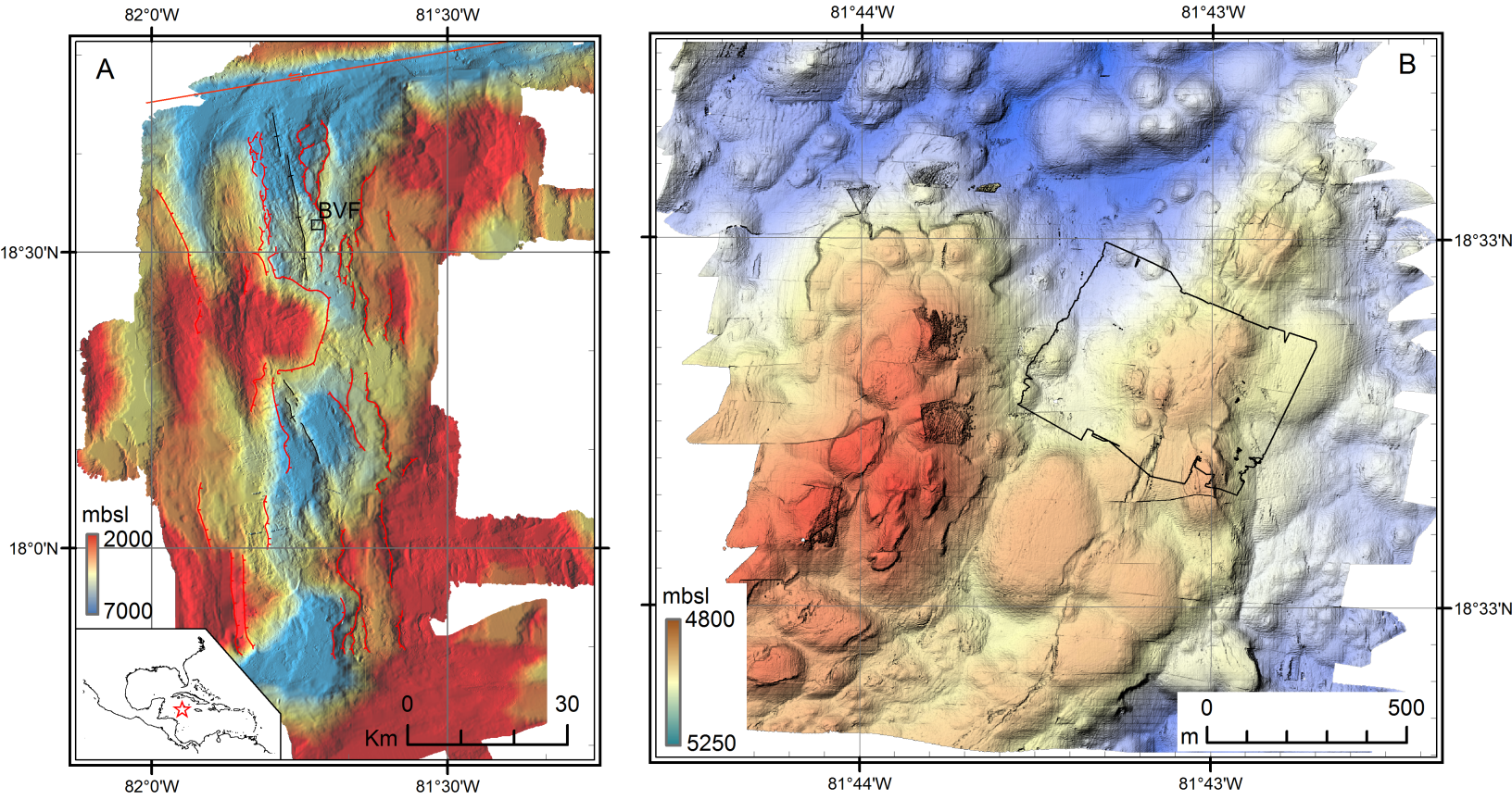

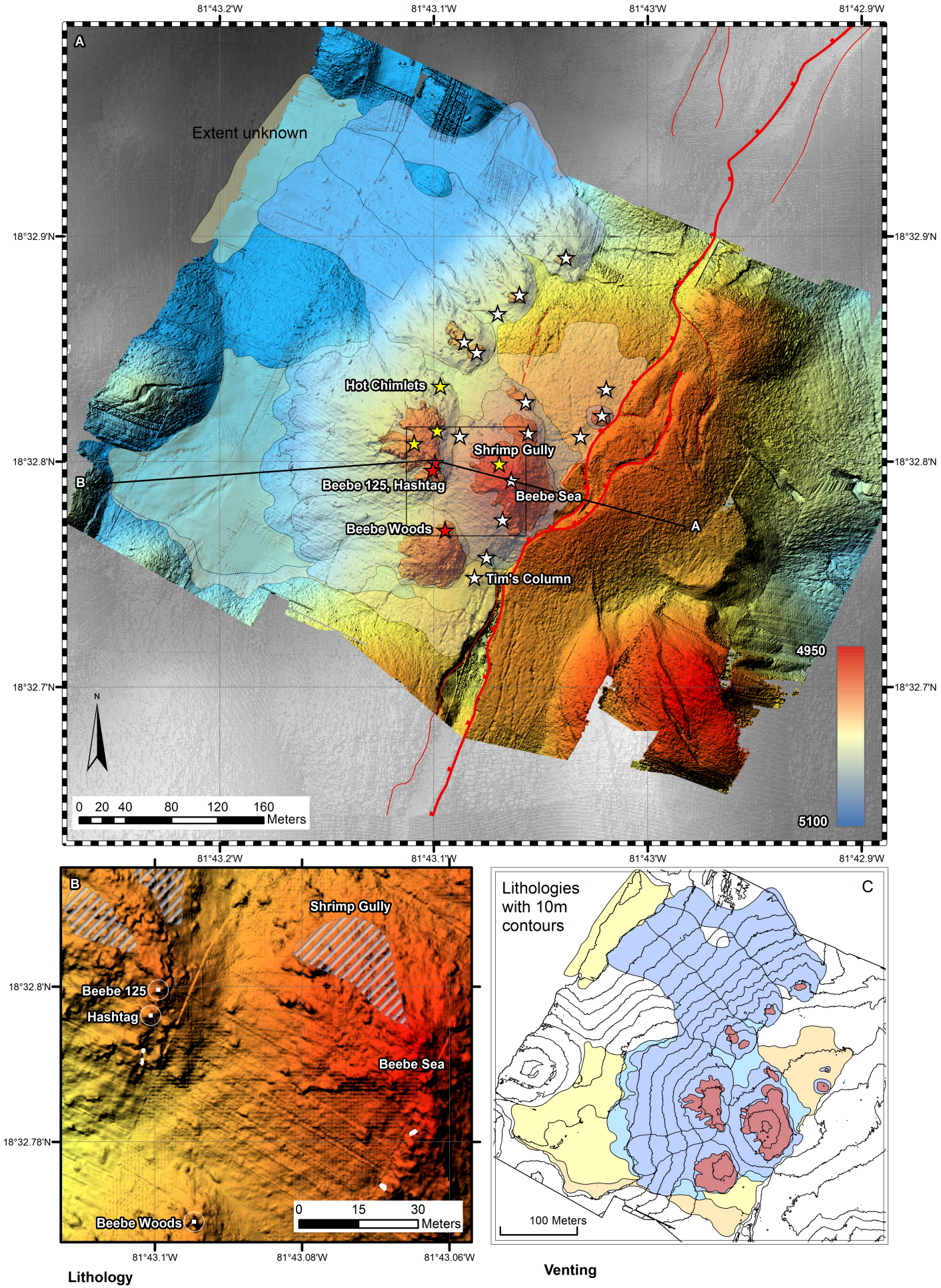

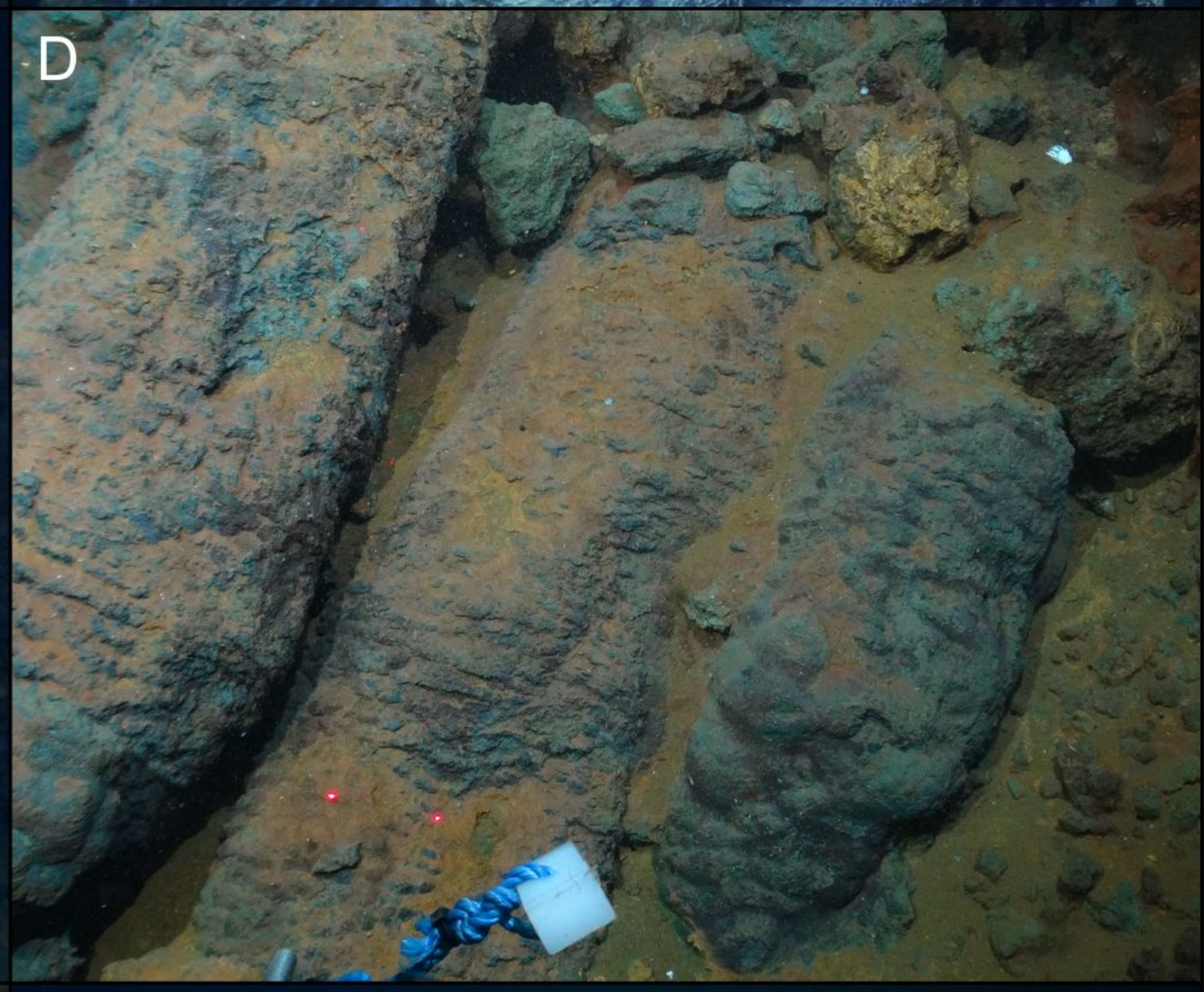

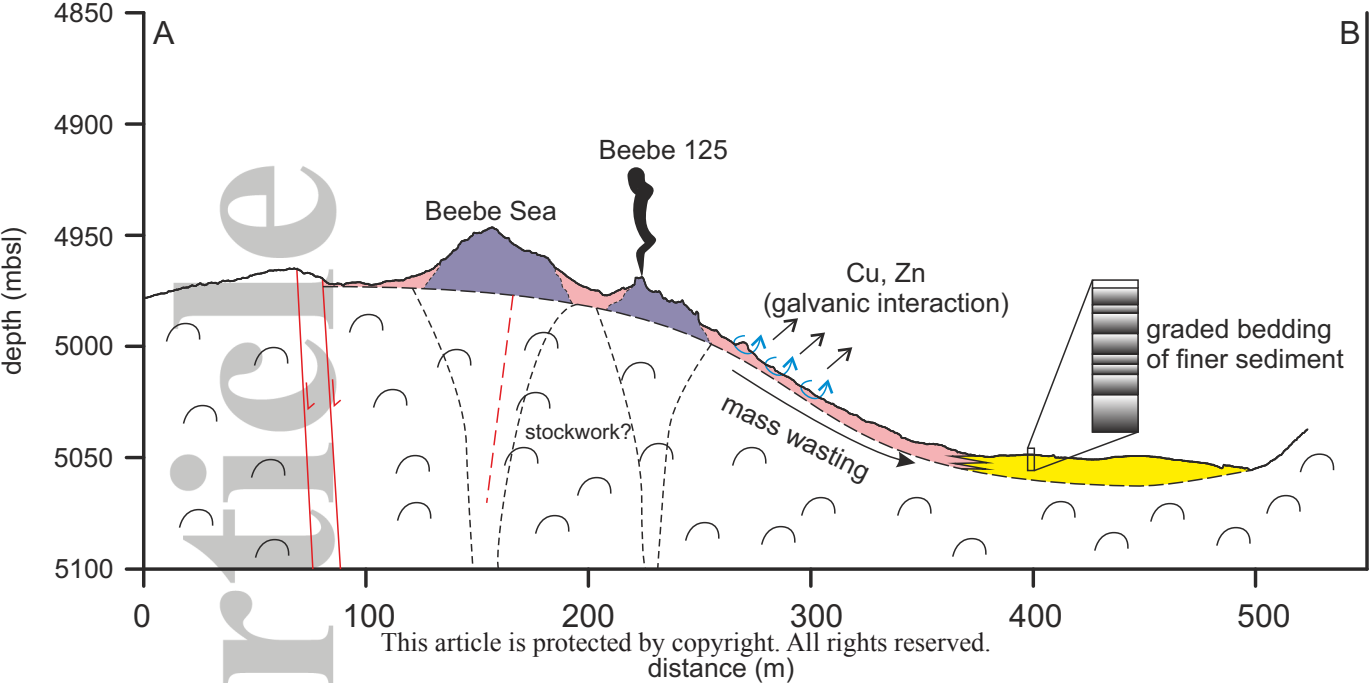

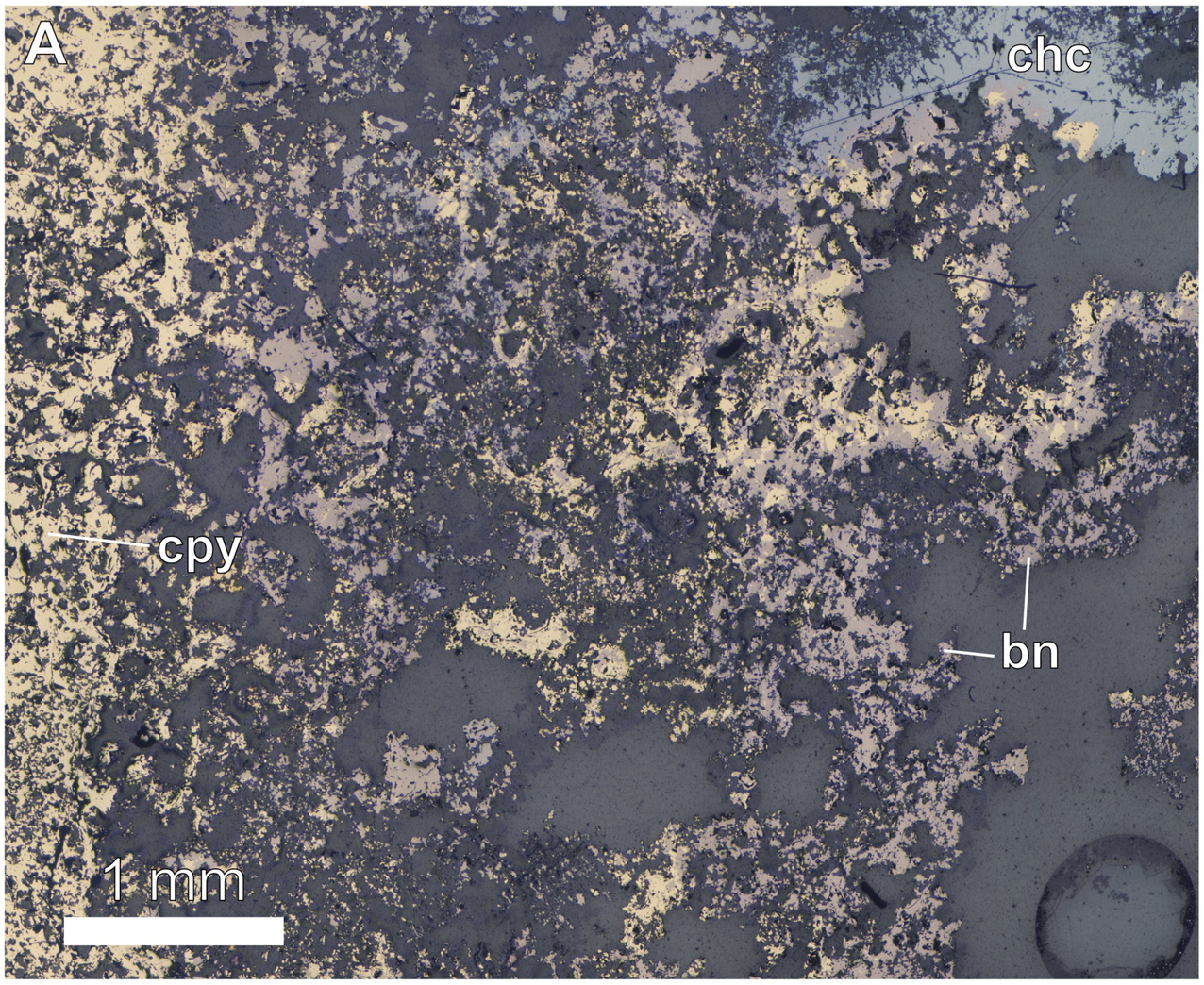

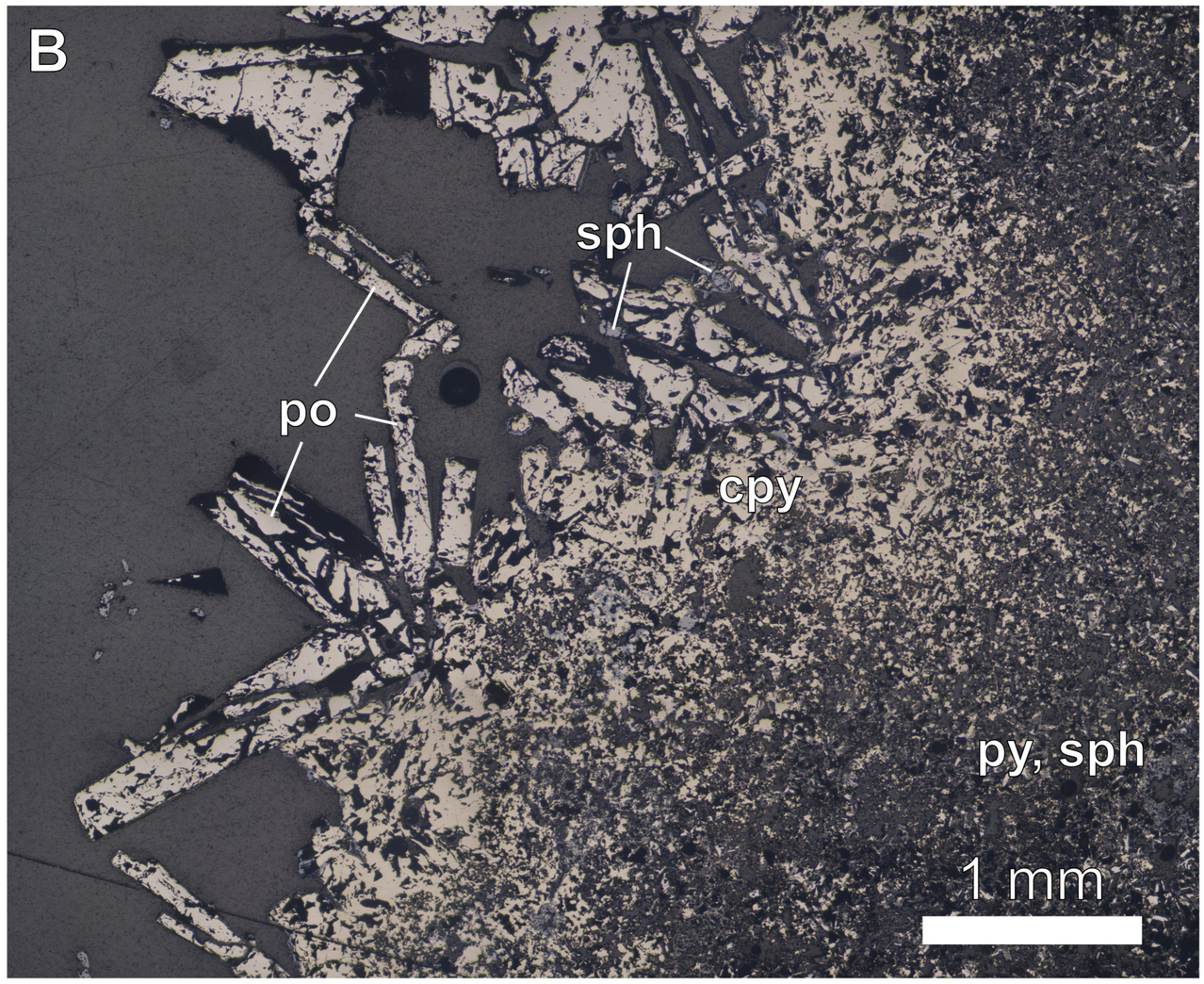

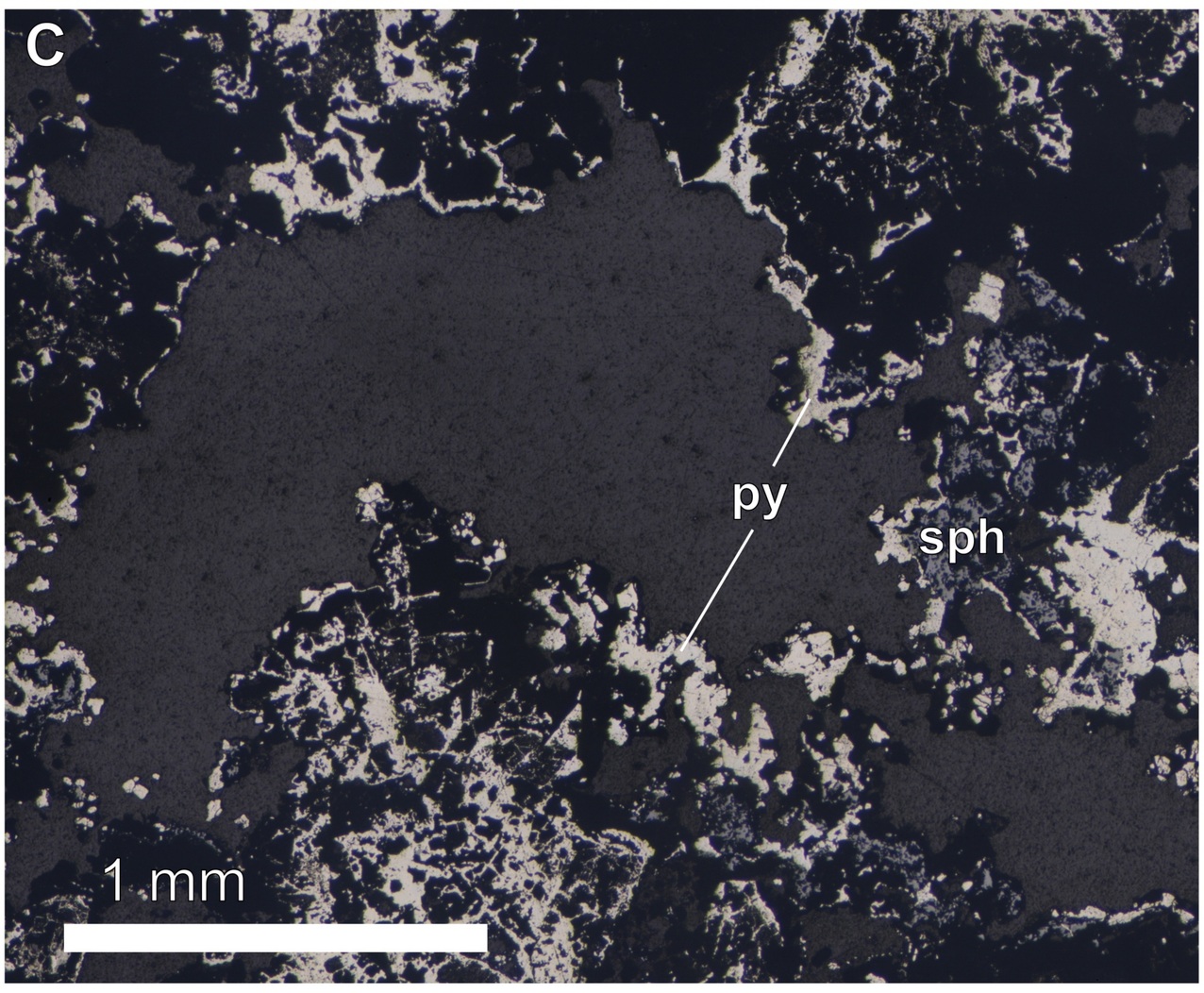

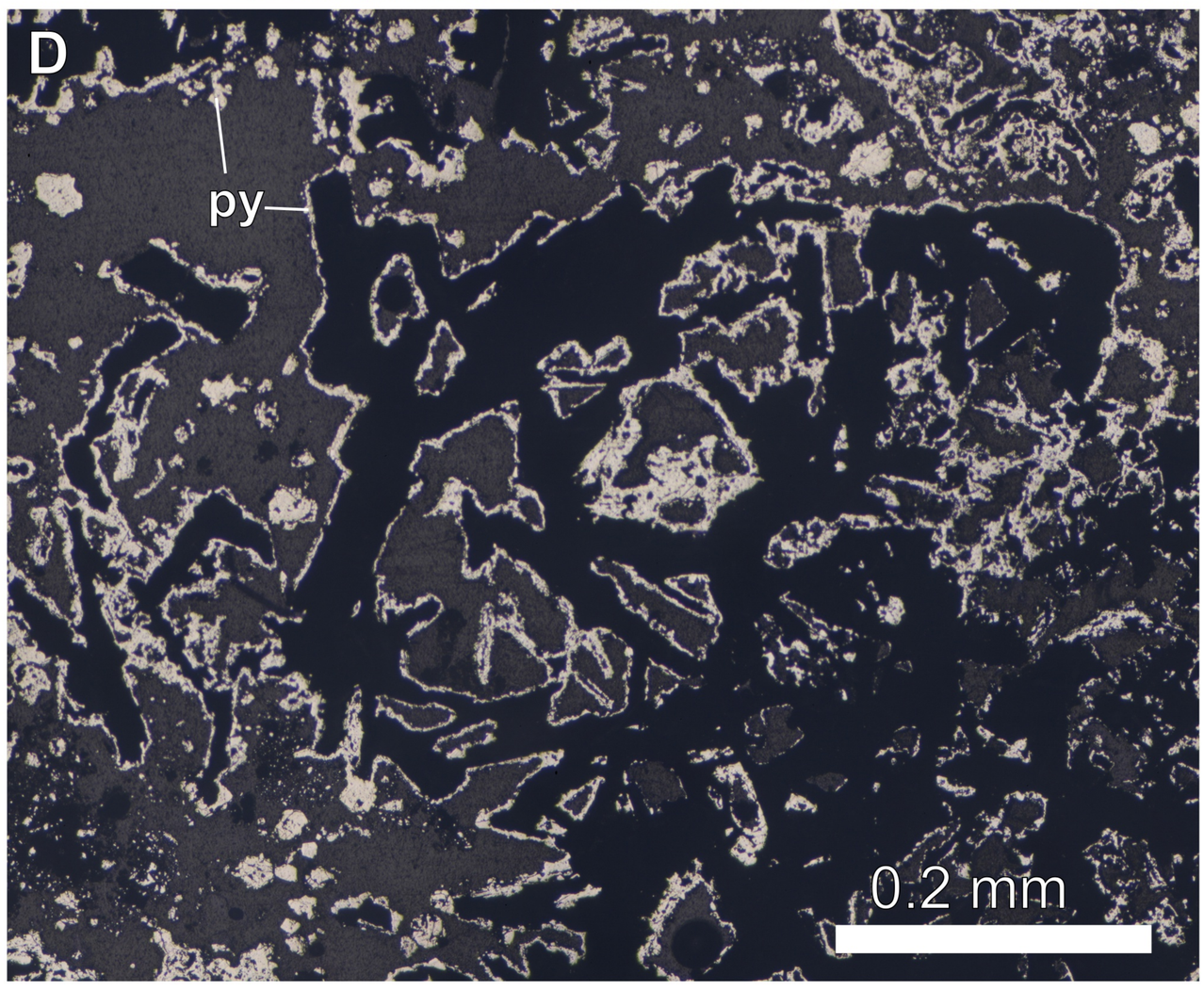

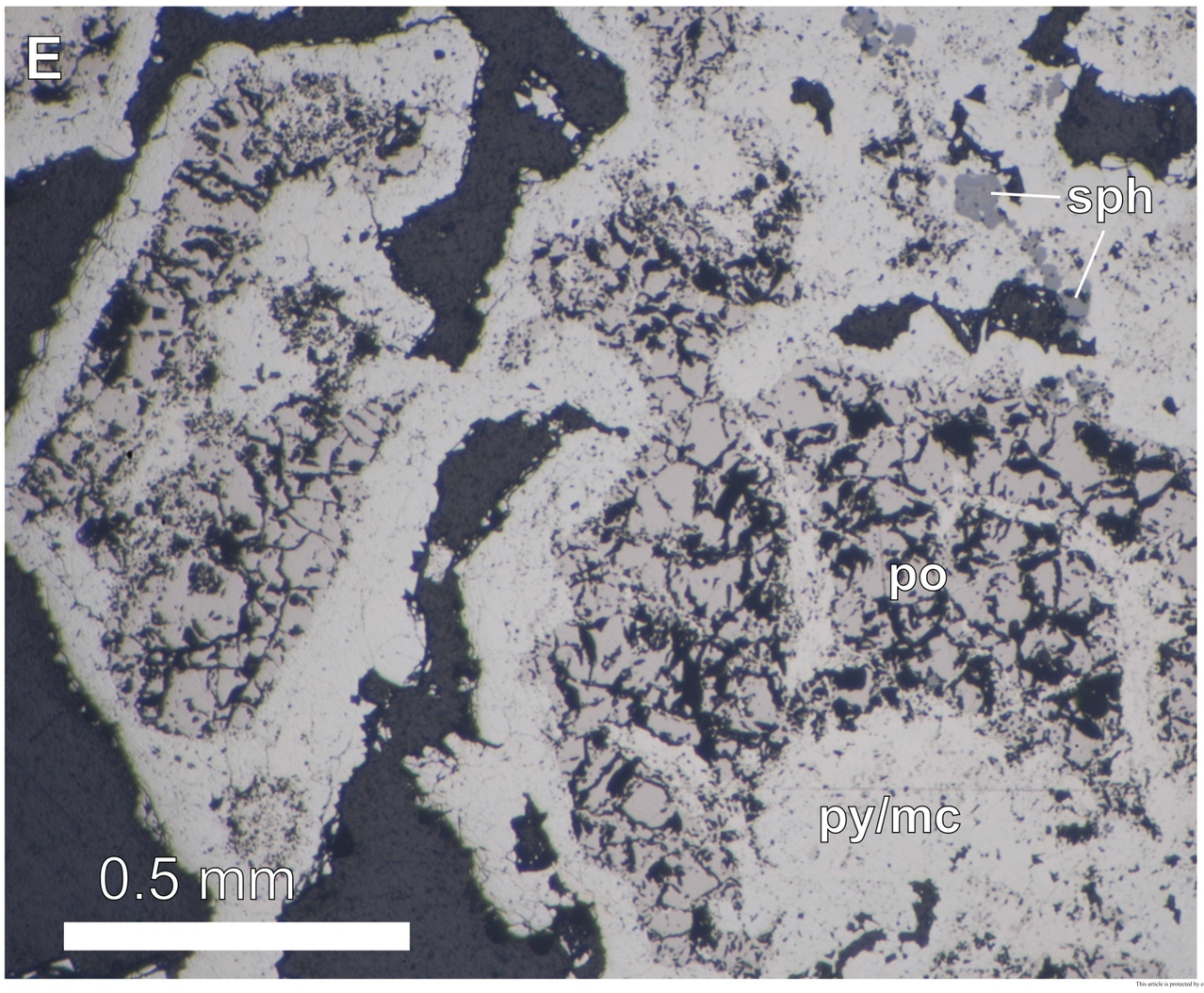

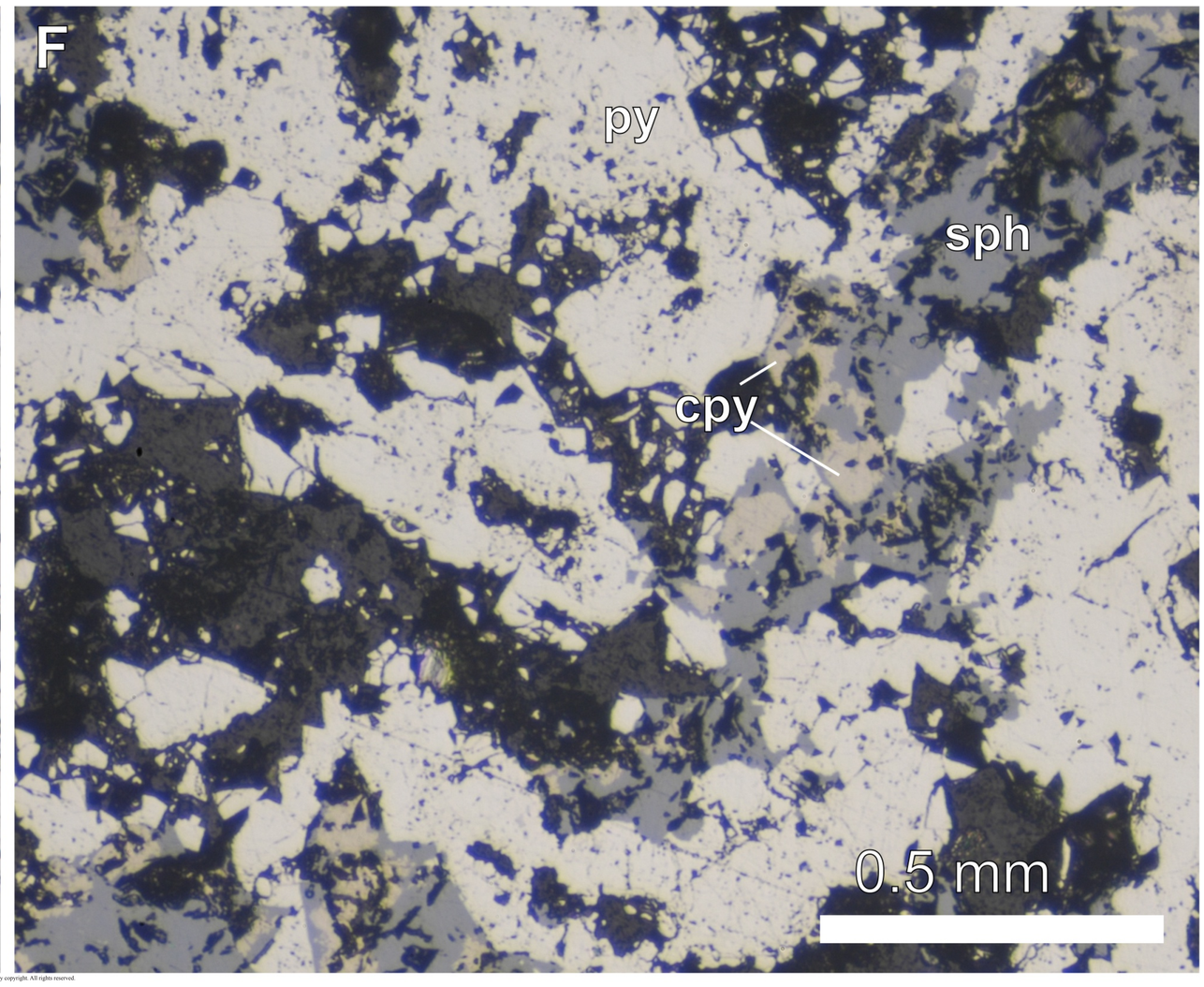

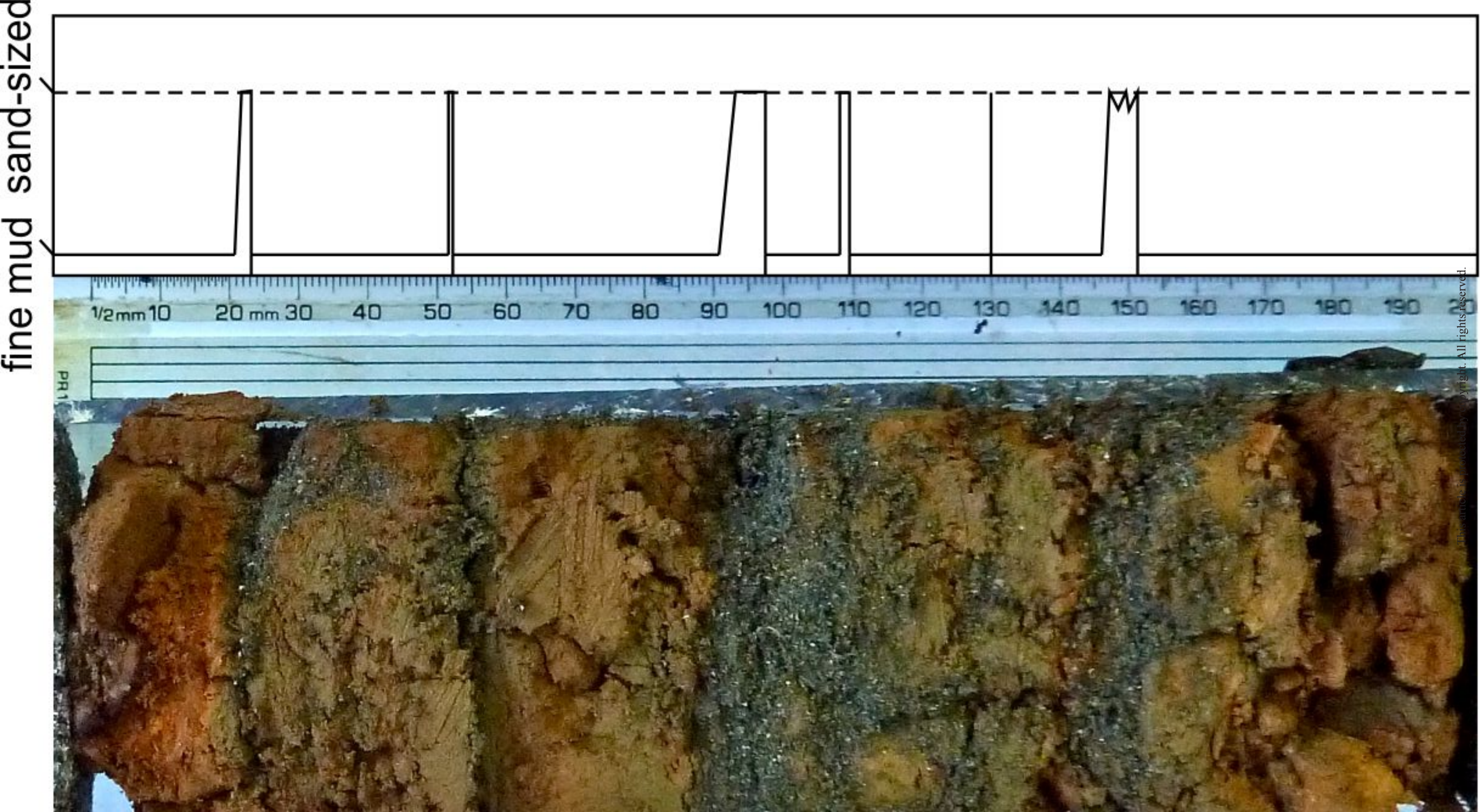

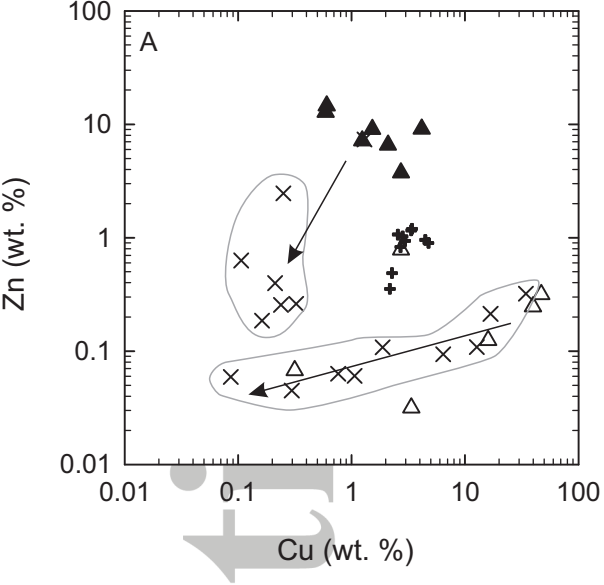

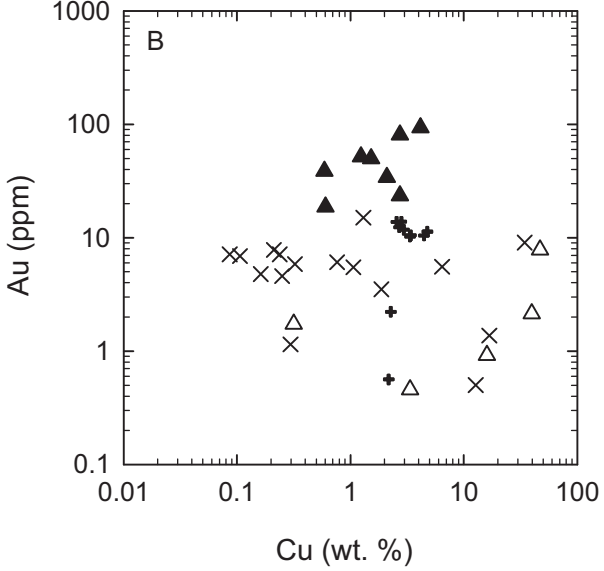

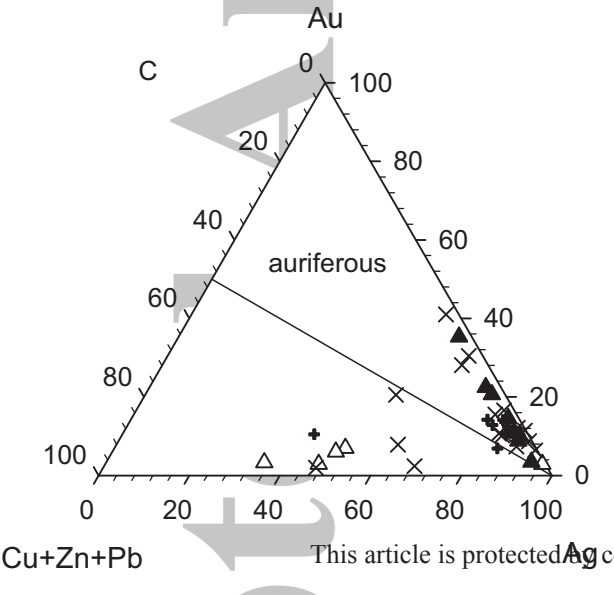

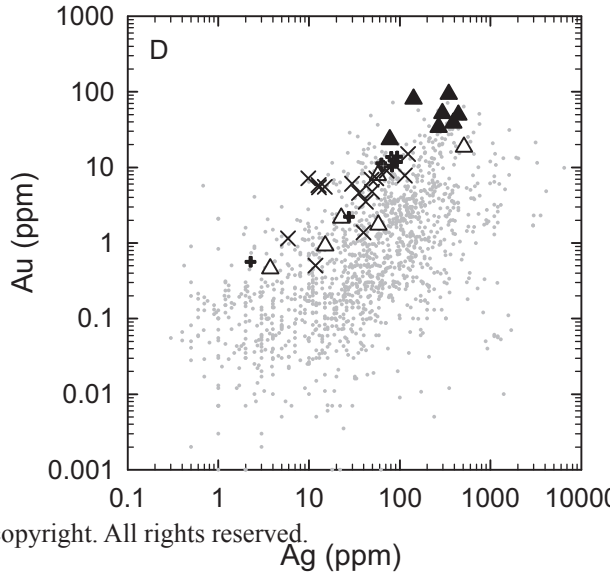

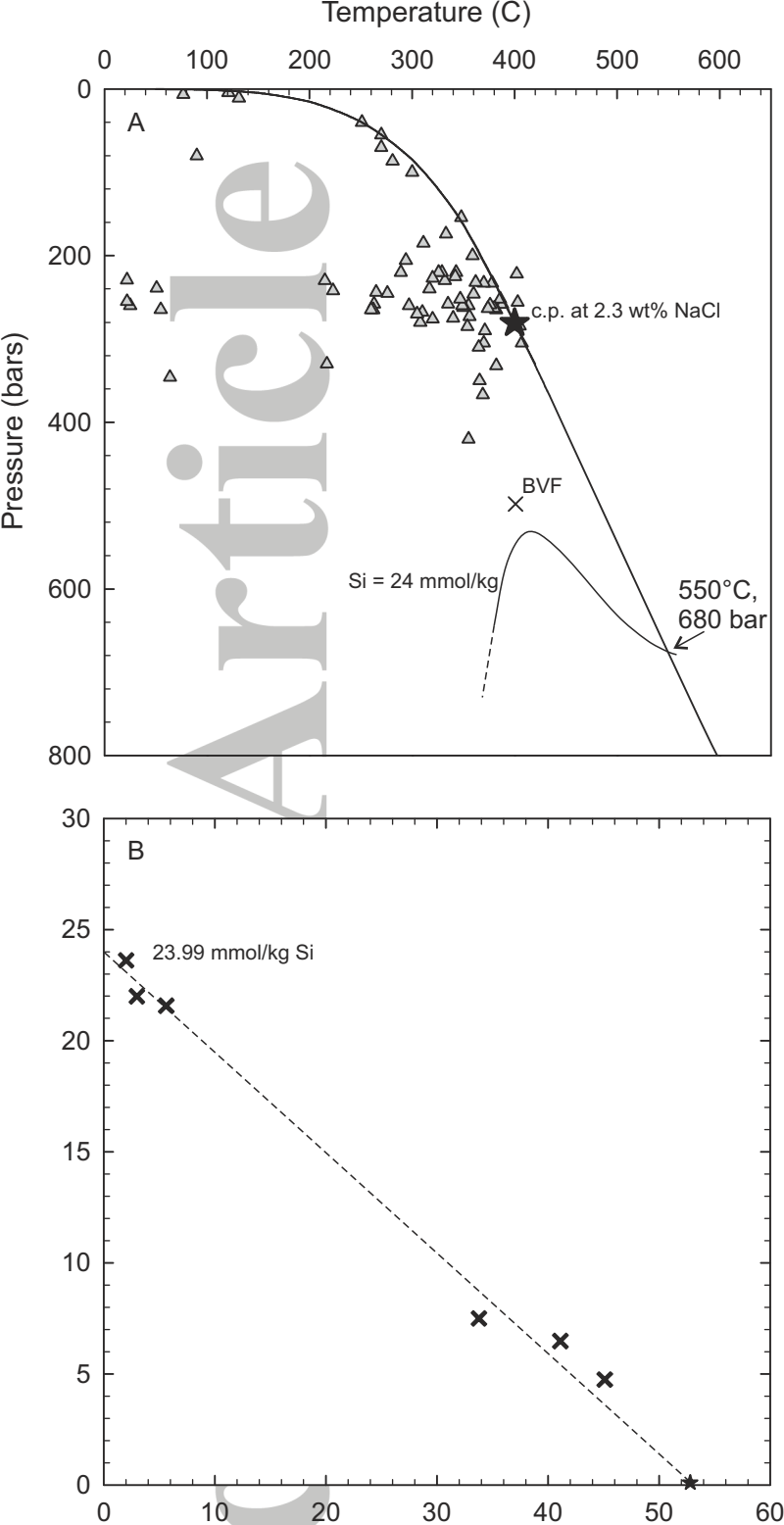

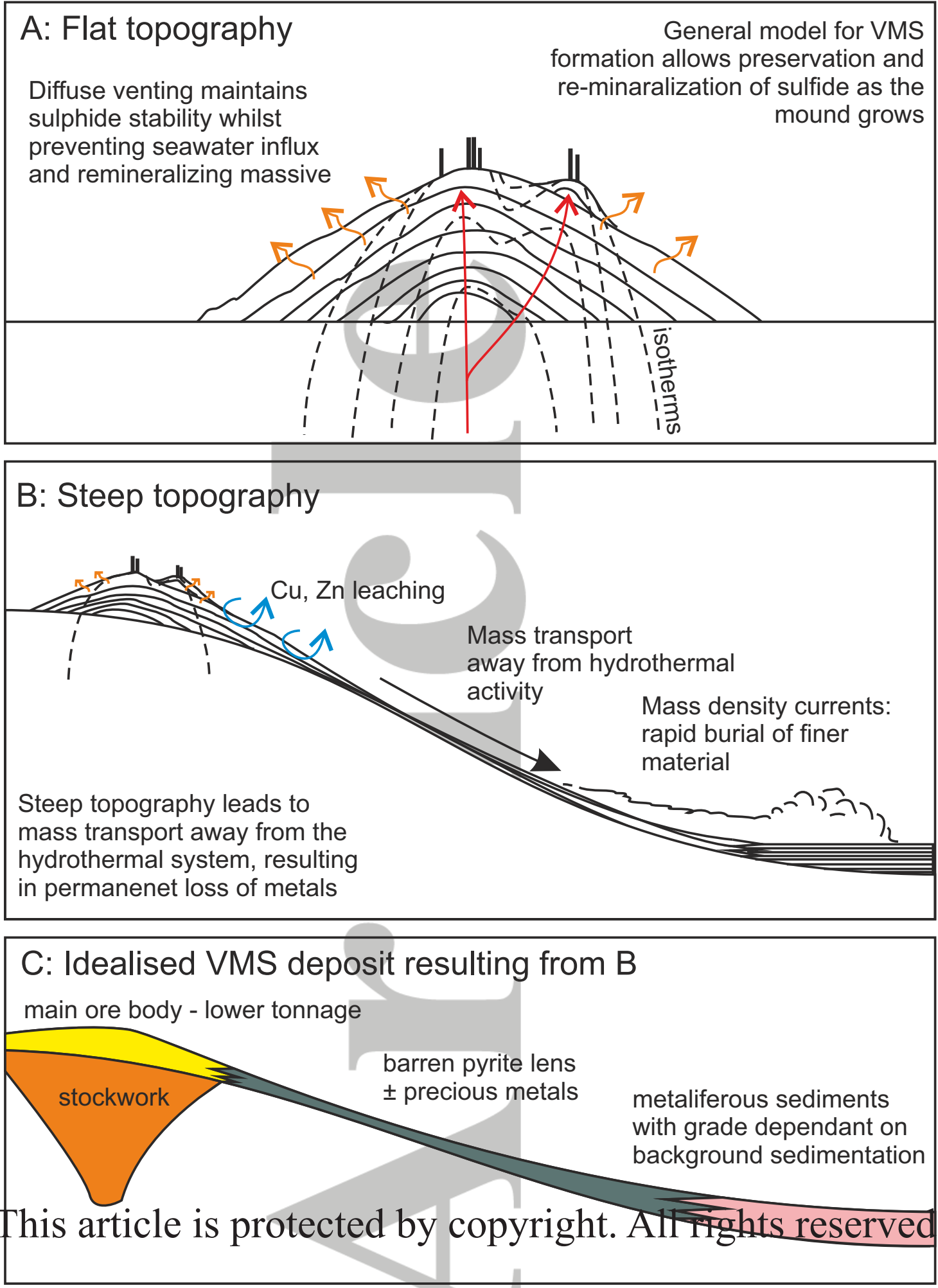

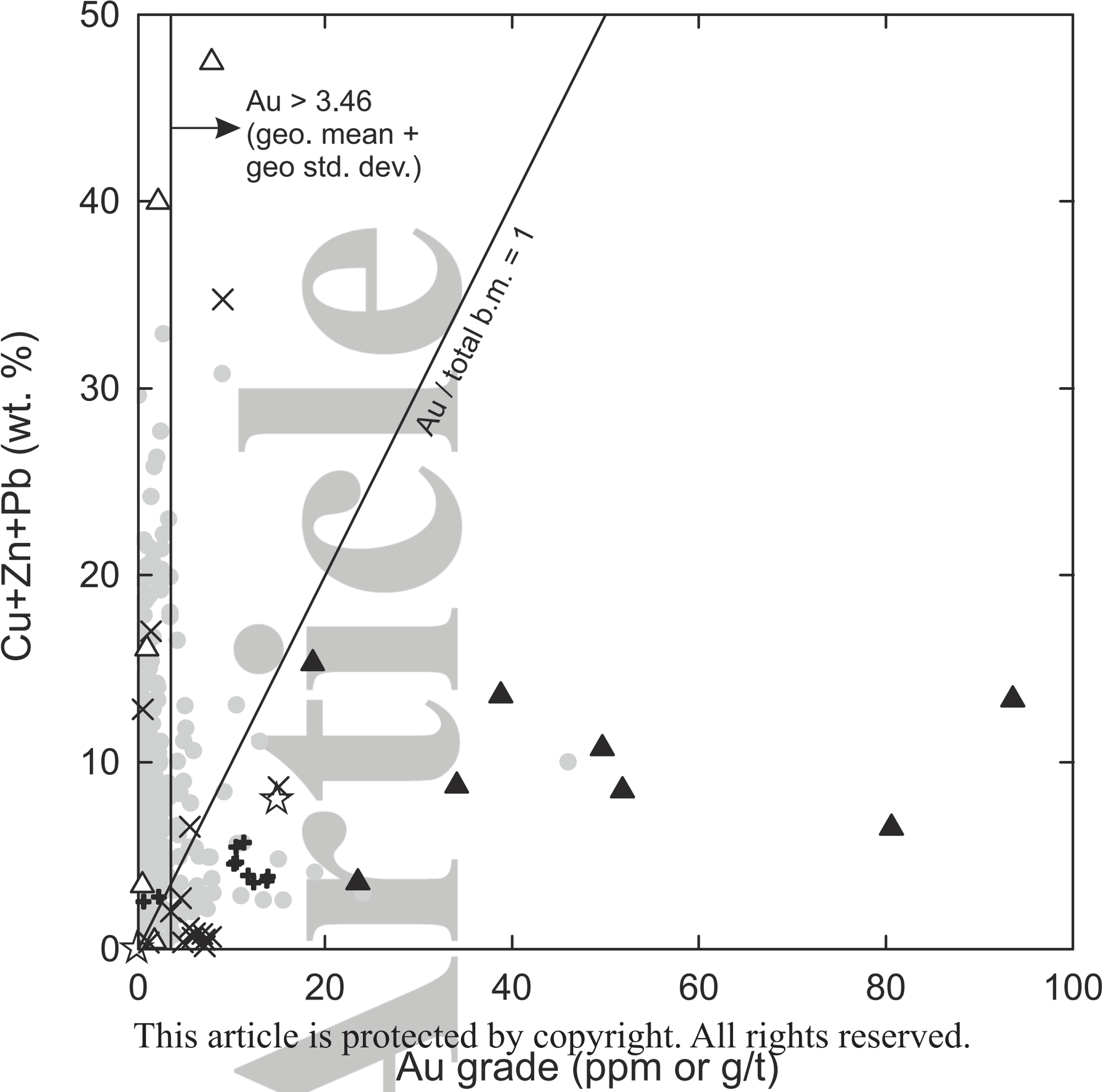

Table 1: Bulk rock geochemical analyses for BVF sulphides

Sample	Type	Fe wt%	Zn wt%	Cu wt%	
64	chimney		5.53	0.031	3.36
67	chimney		14.9	0.124	15.9
69	chimney (extinct)		30.8	0.067	0.316
80	chimney		28.5	0.246	39.7
93	chimney		23.9	0.317	47.1
56	massive sulphide		39.1	0.213	16.8
60	massive sulphide		48.3	0.108	1.88
66	massive sulphide		46.9	0.06	1.06
68	massive sulphide		32.7	0.094	6.44
73	massive sulphide		47	0.631	0.106
74	massive sulphide		45.4	0.398	0.212
75	massive sulphide		45.7	2.46	0.25
77	massive sulphide (solid chalcopy		33.6	0.321	34.4
78	massive sulphide		47.5	0.044	0.297
79	massive sulphide		45.5	0.059	0.086
81	massive sulphide		44.6	0.261	0.325
82	massive sulphide		45.8	0.255	0.239
88	massive sulphide		42.1	7.35	1.3
89	massive sulphide		31.3	0.109	12.7
92	massive sulphide		43.4	0.063	0.761
94	massive sulphide		46.5	0.186	0.162
58	beehive chimney		26.6	9.12	4.15
61	beehive chimney		47.9	3.75	2.72
62	beehive chimney		36.5	9.08	1.52
63	beehive chimney		43.5	7.19	1.24
71	beehive chimney (extinct)		16.2	14.6	0.603
72	beehive chimney		44.7	6.57	2.09
87	beehive chimney (extinct)		33.2	0.782	2.73
90	beehive chimney (extinct)		9.82	12.9	0.59
Core 206-Z3	sediment (depth in mm)				
R7		2	43.9	0.354	2.17
R1		9	39.4	0.897	4.77
R2		43	40.6	1.2	3.41
R3-1		75	42	1.03	2.81
R3-2		75	43.1	0.829	2.69
R3-3		75	42.5	0.939	2.96
R4		94	38.7	1.16	3.36
R5		135	34.8	1.07	2.55
R6		152	32.3	0.487	2.28
R8		192	35.4	0.956	4.46
Error			2%	2%	1%

Footnote: Cu, Fe, Zn analysed by ICP-AES and given in wt. %. All other elements analysed by ICP-MS and giv

Li	Na	K	Rb	Cs	Mg	Ca	Sr	Ba	
0.338	3160	164	0.088	0.008	14600	174000	1560	5.4	
0.787	1030	105	0.037	0.009	13900	125000	1360	9.79	
0.987	6620	529	0.497	0.144	1120	643	17.5	19.8	
0.063	1430	69.9	0.023		2320	5920	42.8	51.8	
0.016	1050	72.4	0.024		1380	3420	43.5	0.269	
4.03	2520	333	0.323	0.032	2240	295	3.19	4.76	
0.112	2300	156	0.068	0.017	346	186	3.52	0.73	
0.061	1880	149	0.084	0.023	275	201	2.85	1.02	
0.154	10600	520	0.656	0.084	1300	520	7.5	0.178	
0.038	1380	171	0.199	0.169	249	411	7.18	0.781	
0.023	1250	120	0.12	0.031	194	79.5	3.01	0.654	
0.207	1230	92.2	0.123	0.053	206	6560	147	3.03	
0.025	374	86.9	0.034		236	287	3.22	0.273	
	1140	126	0.087	0.023	173	607	11	0.908	
0.015	1660	97.1	0.061	0.023	213	158	1.54	0.283	
0.157	4650	310	0.419	0.244	1130	1540	30.8	2.55	
0.048	2850	219	0.382	0.305	376	294	3.05	0.368	
0.075	2230	147	0.113	0.022	505	2910	40.7	1.22	
0.286	2480	151	0.147	0.046	28800	194	2.02	0.286	
0.032	2810	189	0.177	0.096	447	310	2.78	3.67	
0.069	1620	135	0.1	0.03	349	777	15.9	1.37	
0.094	2360	273	0.656	0.197	295	229	2.06	0.182	
0.094	1980	169	0.228	0.055	312	288	4.19	0.086	
0.238	2900	256	0.43	1.12	435	255	3.45	0.238	
0.119	3890	184	0.103	0.039	417	125	2.01	0.223	
0.202	4150	478	0.742	0.096	889	292	5.62	16.4	
0.186	2570	234	0.364	0.381	284	266	2.92	0.227	
0.069	4110	369	0.912	0.337	570	381	3.05	0.092	
0.664	5280	469	0.485	0.059	6700	172000	4690	8.74	
0.651	8180	87.4	0.259	0.031	1920	666	14.2	1.97	
0.961	5550	423	0.845	0.099	3740	416	12.2	2.93	
0.396	3460	475	0.61	0.066	1290	406	10.2	1.45	
0.318	3880	1020	0.736	0.066	885	201	19.8	0.979	
0.256	3490	826	0.648	0.059	766	224	14.8	0.81	
0.201	3760	898	0.665	0.061	551	171	16.5	0.726	
0.688	4480	520	0.819	0.098	3130	401	11.8	2.19	
0.725	5400	986	0.881	0.074	4900	473	18.8	1.9	
3.68	7790	1590	4.04	0.326	4070	1220	24	15	
1.51	4910	329	1.37	0.14	2440	885	5.03	5.31	
4%	4%	4%	4%	3%	4%	5%	4%	4%	

ven in ppm. Sediment samples are taken from the stratified core shown in Figure 6. Samples with missing l

Y	U	Ti	Zr	V	Nb	Cr	Mo	Mn	
0.08	0.169	2.19	0.024	0.273	0.016	0.233	2.69	11.8	
0.066	1.06	0.056	0.009	0.171	0.019	0.19	2.03	17.8	
0.947	5.52	11.8	1.08	92.2	0.12	4.1	93.3	6550	
0.039	1.09	0.672	0.007	0.498	0.015	0.427	1.86	7.23	
0.024	1.4	0.277	0.016	0.594	0.024	0.285	4.05	5.27	
1.2	6.5	1780	2.07	32.2	2.23	31.1	27.7	68.3	
0.051	7.37	2.34	0.077	9.6	0.24	1.85	101	570	
0.076	17.1	1.19	0.099	8.7	0.26	1.26	72.3	885	
0.007	0.425		0.023	1.61	0.015	0.448	57.2	10.9	
0.084	16	3.45	0.084	4.91	0.352	1.34	89.2	1370	
0.031	13.6	1.83	0.031	0.965	0.199	0.59	35.2	1870	
0.069	22.6	4.34	0.238	5.64	0.314	0.751	74.4	707	
0.017	0.392	2.36	0.025	1.34	0.042	0.307	7.98	6.45	
0.047	9.98	2.59	0.039	1.93	0.613	1.06	80.8	997	
0.015	3.43	1.26	0.03	1.61	0.068	0.467	13.2	761	
0.131	7.26	0.524	0.262	9.27	0.017	2.8	64.7	1300	
0.013	4.56	2.57	0.083	3.92	0.013	1.76	62.8	638	
0.255	6.31	4.43	0.3	28.9	0.248	4.57	76.3	579	
0.038	0.626	1.27	0.1	0.263	0.124	0.34	50.9	41.7	
0.08	9.93	0.562	0.096	7.74	0.241	2.9	83.7	1860	
0.084	20.2	2.47	0.108	7.21	0.076	1.49	90.5	3760	
0.007	0.466	2.08	0.087	1.13	0.094	0.525	44.6	22.1	
	0.353	2.21	0.055	0.715	0.039	0.385	29	13.6	
0.009	1.62	0.658	0.064	2.04	0.045	0.64	30.5	21.2	
	0.358	0.676	0.031	0.764	0.039	0.485	29	21.9	
0.016	0.524	1.24	0.04	1.81	0.016	0.403	25.5	30.6	
0.008	0.68	1.86	0.032	1.56	0.016	0.599	27.6	21.6	
	0.567	1.51	0.023	0.506	0.007	0.406	23.5	13.7	
1.47	2.52	11	1.74	56.9	0.4	16.9	14.2	157	
0.808	23.1	15.7	0.314	34.3	0.062	2.27	88.2	82.7	
0.655	13.2	49.9	1.09	85.6	0.232	7.53	154	414	
0.379	8.59	30.7	0.627	41.2	0.107	4.97	113	806	
0.276	5.56	18.7	0.343	36.4	0.075	4.35	111	776	
0.23	5.21	12.2	0.452	33.9	0.068	4.28	113	812	
0.201	4.8	11.6	0.228	30.6	0.061	3.89	104	784	
0.549	9.29	41.3	0.664	58.4	0.172	5.86	133	671	
0.922	13	35.6	0.906	109	0.173	6.74	137	435	
2.15	12.4	230	4.18	157	1.11	15.3	142	217	
1.04	13.7	108	1.9	95.2	0.436	10.1	142	517	
5%	5%	4%	4%	4%	5%	4%	6%	4%	

ocation data were unidentified fragments of other samples, and designated sample numbers aboard ship.

Co	Ni	Ag	Au	Cd	Al	Ga	Sn	Pb	
162	0.724	3.76	0.458	0.684	537	4.21	1.78	4.02	
300	5.01	15.1	0.92	1.19	3.23	1.83	9.23	6.34	
3.83	18.2	58.1	1.73	0.433	482	2.01	9.27	206	
555	46	22.6	2.14	0.625	14.7	2.11	13	2.13	
403	50	57.5	7.85	1.24	34.8	3.27	19.5	8.57	
759	16.8	39.9	1.37	3.84	9780	12.9	11.2	27.6	
165	3.27	42.3	3.51	0.91	41.7	1.09	24.8	81.5	
139	0.819	12.9	5.47	1.09	43.7	2.28	11.7	54	
7.39	0.849	15	5.55	2.03	4.18	9.28	12.9	14.2	
107	1.86	49	6.88	12	157	3.29	17	562	
182	0.893	113	7.79	10.1	39.1	1.8	14.7	276	
100	1.19	35.7	4.59	58.1	302	9.69	49.7	123	
881	0.153	71.8	9.07	5.24	16.9	12.3	61.6	6.6	
221	1.41	5.88	1.15	1.38	13.9	0.239	10.3	84.2	
84.8	0.421	55.3	7.14	1.81	5.34	0.306	39.6	90.3	
1.82	2.88	12.8	5.84	8.93	28.4	1.39	9.62	114	
113	7.92	9.78	7.15	8.84	42.6	1.33	4.23	85.6	
106	2.45	124	15	207	454	36.7	193	156	
73.6	0.324	11.8	0.502	1.72	101	5.96	1.28	3.07	
943	6.04	29.8	6.09	1.55	18.7	0.434	6.35	127	
63.2	16.8	49.5	4.78	2.74	25.1	0.923	14.3	174	
239	1.31	347	93.6	323	362	90.2	321	744	
33.2	0.825	141	80.6	152	583	58	77.4	166	
202	1.01	443	49.7	285	1030	85.4	29.4	1440	
42.3	0.939	296	51.8	266	458	80.9	127	516	
9.34	2.13	509	18.7	562	900	112	747	839	
418	0.866	268	34.1	226	1120	73.9	145	733	
557	6.32	77.7	23.5	89.8	292	6.52	68.7	347	
27.5	9.16	389	38.8	331	1170	36.5	195	1160	
60	2.76	2.27	0.565	11.6	460	1.27	3.07	57	
140	3.83	62.7	11.3	20	1330	16	11.8	265	
107	3.05	81.9	10.5	30.4	746	12.2	22	350	
107	2.89	93.3	13.9	24.8	494	11.1	27	288	
96	2.59	85.4	12.3	22.3	386	10.6	23.1	261	
99.8	2.42	93.1	11.8	26.1	366	11.4	24.4	271	
103	3.64	82.4	10.3	30.5	1070	13	17	344	
83.8	3.37	80.2	13.8	29	1050	20.6	15.7	319	
65	6.21	27.5	2.23	12.5	5010	14.6	13.8	280	
122	5.48	65.7	10.5	21	2370	14.8	21.4	359	
4%	5%	4%	9%	10%	4%	4%	8%	4%	

Bi	Sb	Se
2.32	0.064	36
4.04	0.133	348
0.024	3.35	7.05
2.8		822
4.46	0.578	673
4.61	1.27	181
5.13	6	32.2
2.11	1.94	14.2
0.023	0.949	118
0.016	8.22	1.64
0.161	6.58	2.35
11.2	1.92	399
0.303	0.804	5.76
0.276	1.29	6.02
0.061	1.88	1.97
0.125	2.12	2
0.72	28.1	16.4
1.75	0.201	93.6
0.313	5.15	16.6
0.015	3.87	4.13
1.11	75.1	64.2
0.007	27.2	43.5
0.393	49.5	24.4
0.008	94	2.54
0.947	40.5	41.4
0.912	19.7	39.6
0.008	40.6	9.1
0.157	2.81	6
3.4	13	87.9
2.33	12.6	61.9
2.78	10.7	64.8
2.66	10.1	60.3
3.09	11.3	65.8
2.91	12.2	62
2.96	20.6	60.6
2.33	11.9	40.8
2.45	13.7	61
4%	7%	4%

Table 2: Parameters used in metal content calculation

	Value	Value (conservative)	Units
Input parameters			
Sulphide Volume	218000		m^3
Density of pyrite	5.01		g/cm^3
Porosity	30		%
Copper content	3		wt. %
Au content	7	2	ppm
Calculated:			
Tonnage	0.76		Million tonnes
Copper	22,936		tonnes
Gold	172,635	49,324	oz

Source
Kinsey and German 2014
e.g. Tao et al. 2013
Estimated from sediment samples
Estimated from sediment samples